Energy Reports 10 (2023) 4447–4464

Contents lists available at ScienceDirect

Energy Reports

journal homepage: www.elsevier.com/locate/egyr

Research paper

Parametric estimation of photovoltaic systems using a new multi-hybrid evolutionary algorithm

Pankaj Sharma [a], Saravanakumar Raju [a], Rohit Salgotra [d,e,*], Amir H. Gandomi [b,c,**]

[a] School of Electrical Engineering, Vellore Institute of Technology, India
[b] Faculty of Engineering and Information Technology, University of Technology Sydney, NSW 2007, Australia
[c] University Research and Innovation Center (EKIK), Óbuda University, 1034, Budapest, Hungary
[d] Faculty of Physics and Applied Computer Science, AGH University of Kraków, Poland
[e] Faculty of Information Technology, Middle East University, Amman 11813, Jordan

ARTICLE INFO

Keywords:
Meta-heuristic optimization techniques
Solar PV
CEC 2019 benchmark
HFGD algorithm
Parameter estimation

ABSTRACT

Integrating solar photovoltaic (PV) systems into the modern power grid introduces a variety of new problems. The accurate modelling of PV is required to strengthen the system characteristics in simulation environments. Modelling such PV systems is reflected by a nonlinear I–V characteristic curve behaviour with numerous unknown parameters because there is insufficient data in the cells' datasheet. As a result, it is always a priority to identify these unknown parameters. To extract features of solar modules and build high-accuracy models for modelling, control, and optimization of PV systems, current–voltage data is required. A hybrid evolutionary algorithm is proposed in this paper for precise and effective parameter estimation from experimental data of various PV models. The proposed algorithm is named as hybrid flower grey differential (HFGD) algorithm and is based on the hybridization of flower pollination algorithm (FPA), grey wolf optimizer (GWO), and differential evolution (DE) algorithm. For performance evaluation, CEC 2019 benchmark data set is used. To increase the accuracy of the output solutions, we also combined the Newton–Raphson approach with the proposed algorithm. Four PV cells/modules with diverse characteristics, including RTC France Single Diode Model (SDM), RTC France Double DM (DDM), Amorphous Silicon aSi:H, and PVM 752 GaAs Thin-Film, are used to validate the effectiveness as well as the feasibility of the proposed algorithm. The parameter results obtained through the utilization of HFGD algorithm have been compared with other evolutionary algorithms through aspects of precision, reliability, and convergence. Based on the outcomes of the comparison, it has been seen that the HFGD algorithm obtained the lowest root-mean-square error (RMSE) value. Friedman's rank and Wilcoxon test are carried out for the statistical analysis of the proposed work. The I–V and P–V characteristics are drawn along with the box plot for different PV cells/modules. Statistical and experimental results show the superiority of the proposed algorithm with respect to its counterpart.

1. Introduction

De-carbonization has established a consensus among nations attributed to the growing global temperature, and the clean replacement of fossil fuels with solar, wind, wave, tidal, hydro, nuclear, etc. power on the generating side is vital to attaining this objective. Future power systems will predominantly depend on new energy sources (Chen et al., 2023). PV systems are one of the proposed alternatives to obtain this clean replacement of fossil fuels (Abbas et al., 2023; Sharma et al., 2022a). The research on solar cell materials mostly centres around two aspects: the advancement of novel materials, such as perovskites and quantum dots, as well as the enhancement of existing materials, including as silicon, through optimization techniques (Zhi et al., 2023; Nowsherwan et al., 2023). Researchers are currently employing optimization techniques to enhance the operational effectiveness of solar cells, while concurrently focusing on enhancing the stability and efficiency of perovskite solar cells (Bati et al., 2023; Chowdhury et al., 2023). With the ongoing reduction in the cost of solar cells as well as the continuous enhancement in their efficiency, solar energy is progressively emerging as a feasible alternative for electricity generation because it produces electricity through PV power without inflicting

* Corresponding author at: Faculty of Physics and Applied Computer Science, AGH University of Kraków, Poland.
** Corresponding author at: University Research and Innovation Center (EKIK), Óbuda University, 1034, Budapest, Hungary.
E-mail addresses: pankaj.sharma2020@vitstudent.ac.in (P. Sharma), rsaravanakumar@vit.ac.in (S. Raju), r.03dec@gmail.com, rohits@agh.edu.pl (R. Salgotra), gandomi@uts.edu.au (A.H. Gandomi).

https://doi.org/10.1016/j.egyr.2023.11.012
Received 3 June 2023; Received in revised form 20 October 2023; Accepted 7 November 2023
Available online 16 November 2023

adverse effects on the environment, unlike fossil fuels (Liu et al., 2023; Nyamathulla et al., 2023; Anjaneya Vara Prasad et al., 2023). But, environmental factors such as unpredictable weather, airborne particles, and temperature reduce the efficiency of the PV, large PV grid-connected systems still struggle to provide electricity with great efficiency and precision (Rathod and Subramanian, 2022; Sharma and Naidu, 2022). These challenges can be solved by developing accurate PV models that improve the efficiency and accuracy of solar cell energy conversion (Mo et al., 2023; Nyamathulla and Chittathuru, 2023). The functionality, as well as the efficiency of the models whose parameters are estimated, are known to accurately describe the behaviour of PV panels. For this purpose, it is essential to use a technique for precise parameter estimation that optimizes the energy efficiency of PV models (Jordehi, 2016).

Also, various methods have been reported in the literature to extract solar PV parameters. Each method has its own disadvantages in terms of accuracy, complexity and convergence or speed. They are categorized broadly as analytical, deterministic, and MH optimization techniques. In comparison to alternative approaches for determining PV model parameters, analytical methods are more efficient and user-friendly. But, the solution's dependability and precision are substandard since postulates must be formulated before analysis. Moreover, deterministic strategies may readily get trapped in cycles of local maxima because their underlying assumptions might lead them to be misled. MH optimization techniques are similar to the deterministic methods. MH optimization has some advantages: performance reliability, robustness, simplicity, ease of implementation, etc. The beauty of MH algorithms is that they impose no restrictions on the problem's characteristics. Hence, they can be simply implemented for a broad variety of real-world challenges. Therefore, they have become viable options for fetching PV model parameters (Abbassi et al., 2018; Venkateswari and Rajasekar, 2021).

Many MH algorithms are available in the literature to address this problem such as nuclear reaction optimization (NRO) (Wei et al., 2019), gaining sharing knowledge (GSK) (Xiong et al., 2021), tunicate swarm algorithm (TSA) (Beşkirli and Dağ, 2022), bald eagle search (BES) (Nicaire et al., 2021), teaching–learning based optimization (TLBO) (Rao et al., 2012), hybrid successive discretization algorithm (HSDA) (Cotfas et al., 2021), successive discretization algorithm (SDA) (Cotfas et al., 2019), heap-based optimizer (HBO) (AbdElminaam et al., 2022), generalized oppositional teaching learning-based optimization (GOTLBO) (Chen et al., 2016), improved teaching learning based optimization (ITLBO) (Li et al., 2019b), ranking teaching learning based optimization (RTLBO) (Xiong et al., 2018b), improved whale optimization algorithm (IWOA) (Xiong et al., 2018a), improved JAYA optimization algorithm (IJAYA) (Jordehi, 2018), teaching–learning-based artificial bee colony (TLABC), backtracking search optimization algorithm (BSA), Chen et al. (2018), supply demand based optimization (SDO) (Xiong et al., 2019), harmony search (HS) (Askarzadeh and Rezazadeh, 2012), genetic algorithm (GA), barnacles mating optimizer algorithm(BMOA) (Madhiarasan et al., 2022), enhanced lévy flight bat algorithm (ELBA), directional bat algorithm (DBA), novel bat algorithm (NBA), bat algorithm (BA) (Deotti et al., 2020), improved slime mould algorithm (CNMSMA) (Liu et al., 2021), honey badger algorithms (HBA) (Düzenli et al., 2022), logistic chaotic rao-1 optimization algorithm (LCROA) (Lekouaghet et al., 2021), ali baba and forty theives (ABT) (Sharma et al., 2022b), artificial humming bird Optimization (AHO) (Ayyarao and Kishore, 2023), pheromone value black widow optimization (pv-BWO), hybrid sailfish optimization (h-SFO) (Chauhan and Prakash, 2023), side blotched lizard algorithm (SBLA) (Navarro et al., 2023), bonobo optimizer (BO) (Sharma and Raju, 2023a), squirrel search algorithm (SSA) (Maden et al., 2023), etc. Researchers have presented a list of improved solution approaches that rely on MH algorithms.

Additionally, according to the well-known no-free lunch theorem, any solution method for an optimization problem has the potential for improvement and expansion (Wolpert and Macready, 1997; Hassan et al., 2020; Rauf et al., 2021). So it is necessary to use new optimization techniques to determine the parameter estimation of the solar PV and see how these new algorithms perform. In the present work, we introduce a new hybrid flower pollination algorithm (FPA) (Yang, 2012), grey wolf optimization (GWO) (Mirjalili et al., 2014a) and differential evolution (DE) (Storn and Price, 1997) based (HFGD) algorithm. The new algorithm uses the basic structure of FPA and incorporates changes inspired by GWO and DE into it. The algorithm uses a combination of equations that are best suited and are derived from basic FPA, GWO and DE algorithms. The major reason for using GWO in FPA is to improve the exploration (*expl*) operation and DE based equations helps to improve the exploitation (*expt*) process. For performance enhancement, adaptive parametric operations are performed and a new concept of iterative division is introduced. Apart from these added advantages, the parameters of the proposed algorithm are made self-adaptive in nature.

Accordingly, the paper's main objective is to predict the parameters of SDM, DDM, Amorphous Silicon aSi:H, and PVM 752 GaAs Thin-Film of the solar PV cell/modules by the HFGD algorithm. The accuracy of the proposed HFGD algorithm is evaluated using RMSE. In addition, data from recent MH algorithms are compared with the characteristics derived by HFGD algorithm. Additionally, an improvement in the RMSE values is observed. This paper uses a HFGD algorithm but efficient MH algorithm to address the PV model parameter extraction issue based on the considerations above. Due to the excellent behaviour of the HFGD algorithm, in this paper HFGD algorithm is introduced to the parameter extraction of SDM, DDM, Amorphous Silicon aSi:H and PVM 752 GaAs thin-film are presented. The main contributions of this paper are

- A new algorithm namely HFGD is proposed with the added advantages of FPA, GWO and DE algorithm by incorporating the best equations and parameters of GWO and DE in FPA.
- A new concept of division of iterations is added in the local as well as global search phase of the proposed algorithm, along with adaptive switching probability and significant population adaptation for improved convergence in lesser number of iterations.
- The proposed algorithm is evaluated on CEC 2019 benchmark dataset (Brest et al., 2019; Sharma and Raju, 2023b), statistical tests (Friedman and wilcoxon tests) and is compared with respect to some of the best known algorithms including jDE100, FPA, DE, YDSE, among others.
- HFGD is introduced to solve the parameter extraction of SDM, DDM, Amorphous Silicon aSi:H and PVM 752 GaAs thin-film are presented.
- Comparing the results obtained by the HFGD algorithm with other MH algorithm.

The rest of the paper is organized as: The mathematical modelling of the SDM, and DDM is presented in Section 2. Section 3 demonstrates the fundamentals of nature-inspired algorithms. The detailed process of the HFGD algorithm is introduced in Section 4. In Section 5, experimental results of HFGD algorithm for CEC benchmarks with respect to other MH algorithms are presented. Apart from that, real world parametric estimation of the solar PV system including SDM, DDM, Amorphous Silicon aSi:H and PVM 752 GaAs thin-film cell/module is done. In Section 6, the summary of results, drawbacks, and insightful implications are presented and important conclusion are outlined in the last Section. The outline of this research article is presented in Fig. 1.

2. Mathematical modelling

In the literature, the modelling of PV cells is shown using the SDM and DDM, which are shown in Figs. 2 and 3, respectively. Typically, equivalent circuit are used to illustrate the connection between, I and V of PV cells/modules. The SDM has five unknown parameters, namely R_s, n, I_{sc}, R_{shu}, and I_{Ph}. In contrast, the DDM has two additional parameters (for a total of seven) than the SDM i.e n_2, and I_{sc2}. The next subsections briefly discuss the SDM and DDM to highlight the IV characteristics of PV.

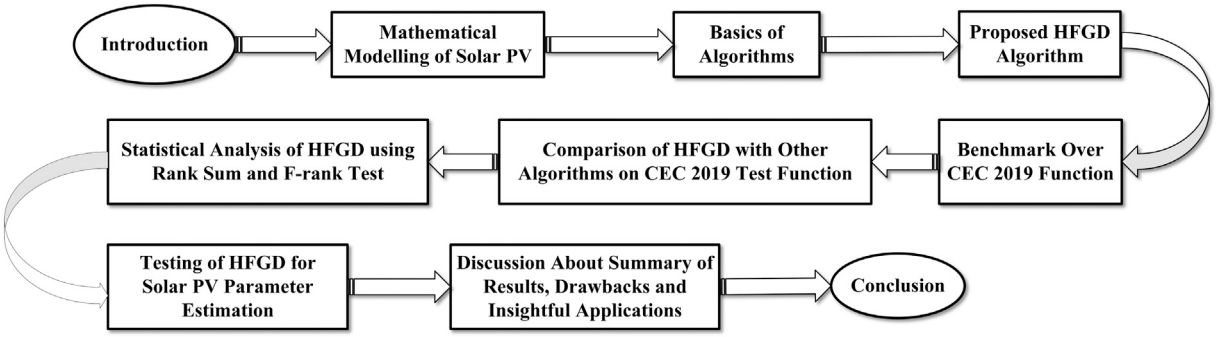

Fig. 1. Outline of the article.

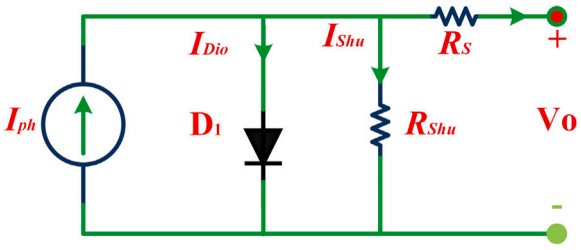

Fig. 2. Equivalent circuit of SDM.

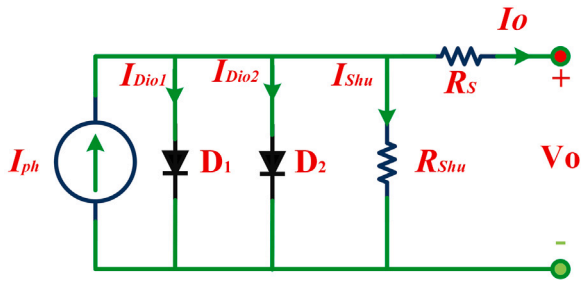

Fig. 3. Equivalent circuit of DDM.

2.1. Single diode model

SDM is a commonly used mathematical model and is illustrated in Fig. 2. The output current (I_o) can be calculated using Eq. (1) given below (Maden et al., 2023; Sharma et al., 2022c; Prasad and Dhanamjayulu, 2021):

$$I_o = I_{Ph} - I_{dio} - I_{shu} \tag{1}$$

The mathematical expressions for the I_{dio} and I_{shu} are given in Eqs. (2) and (3) respectively.

$$I_{dio} = I_{sc}\left[exp\left(\frac{q(V_o + I * R_s)}{nkT}\right) - 1\right] \tag{2}$$

$$I_{shu} = \frac{V_o + I * R_s}{R_{shu}} \tag{3}$$

The I_o is presented in the given Eq. (4).

$$I_o = I_{Ph} - I_{sc}\left[exp\left(\frac{q(V_L + I * R_{shu})}{nkT}\right) - 1\right] - \frac{V_L + I * R_s}{R_{shu}} \tag{4}$$

where, shunt resistance (R_{shu}), diode ideality factor (n), series resistance (R_s), reverse saturate current (I_{sc}), Boltzmann constant ($k = 1.3806503\times 10-23$ J/K), charge of the electron ($q = 1.60217646 \times 10-19$ C), and Kelvin temperature of the solar cell (T). An accurate PV model can be created by extracting these parameters (R_s, n, I_{sc}, R_{shu}, and I_{Ph}).

2.2. Double diode model

It is clear from Fig. 3 that two diodes are added. And, its mathematical formula is given in Eq. (5) (Abdel-Basset et al., 2021; Navarro et al., 2023):

$$I_o = I_{Ph} - I_{dio1} - I_{dio2} - I_{shu} \tag{5}$$

Eqs. (6) and (7) represents the mathematical expressions for the I_{dio1} and I_{dio2}, respectively.

$$I_{dio1} = I_{sc1}\left[exp\left(\frac{q(V_o + I * R_{shu})}{n_1 kT}\right) - 1\right] \tag{6}$$

$$I_{dio2} = I_{sc2}\left[exp\left(\frac{q(V_o + I * R_{shu})}{n_2 kT}\right) - 1\right] \tag{7}$$

The I_o is displayed in the given Eq. (8).

$$I_o = I_{Ph} - I_{sc1}\left[exp\left(\frac{q(V_o + I * R_{shu})}{n_1 kT}\right) - 1\right] - I_{sc2}\left[exp\left(\frac{q(V_o + I * R_{shu})}{n_2 kT}\right) - 1\right] - \frac{V_o + I * R_s}{R_{shu}} \tag{8}$$

where, diode ideality factor (n_1) and (n_2) and reverse saturate current (I_{sc1}) and (I_{sc2}). An accurate PV model can be created by extracting these parameters (R_s, N_1 and N_2, I_{sc1}, I_{sc2}, R_{shu}, and I_{Ph}).

2.3. Objective function

The HFGD algorithm is utilized to solve an optimization challenge in order to identify the parameters of the PV cells/modules model. By addressing this optimization challenge, the fitness function is minimized, leading to the discovery of unknown parameters. The objective of the HFGD is to minimize the error among the calculated current (I_e) and the measured current (I_m). Generally, the error function ($RMSE$) can be expressed as an objective function and given in Eq. (9) (Yang et al., 2023; Abd El-Mageed et al., 2023; Sharma and Raju, 2023a). Six additional statistical indicators are included to demonstrate the accuracy of the developed PV model are presented in Eqs. (10), (11), (12), (13), (14) and (15), respectively.

$$F = \sqrt{\frac{1}{N}\sum_{i=1}^{N}\left[I_m - I_e\right]^2} \tag{9}$$

The individual absolute error $IAE_{current}$ and IAE_{Power} is given in the Eqs. (10) and (11).

$$IAE_{Current} = \sum_{i=1}^{N}\left|I_m - I_e\right| \tag{10}$$

$$IAE_{Power} = \sum_{i=1}^{N}\left|P_m - P_e\right| \tag{11}$$

The Mean Absolute Error (MAE), Relative Error (RE), Mean Bias Error (MBE), Mean Absolute Percentage Error (MAPE), Normalized RMSE

(NRMSE), Normalized MBE (NMBE), Normalized MAE (NMAE), and sum of the squared error (SSE) is given as Eqs. (12), (13), (14) (15), (16), (17), (18), and (19) respectively.

$$RE = \frac{I_m - I_e}{I_m} \tag{12}$$

$$MBE = \frac{1}{N}\sum_{i=1}^{N}\left(I_m - I_e\right) \tag{13}$$

$$MAE = \frac{1}{N}\sum_{i=1}^{N}\left|I_m - I_e\right| \tag{14}$$

$$MAPE = \frac{1}{N}\sum_{i=1}^{N}\left|\frac{I_m - I_e}{I_m}\right| \tag{15}$$

$$NRMSE = \frac{RMSE}{mean\left(I_m\right)} \tag{16}$$

$$NMBE = \frac{MBE}{mean\left(I_m\right)} \tag{17}$$

$$NMAE = \frac{MAE}{mean\left(I_m\right)} \tag{18}$$

$$SSE = \sum_{i=1}^{N}\left(I_m - I_e\right)^2 \tag{19}$$

where, N is the sample number, P_m, P_e are the measured and calculated power, respectively. And also I_m, and I_e, measured as well as calculated current, respectively.

3. Fundamentals of nature-inspired algorithms

This section demonstrates the fundamentals of the algorithms utilized to propose our new hybrid (HFGD) algorithm. The algorithms that are used, such as FPA, GWO, and DE, are described as:

3.1. Flower pollination algorithm

FPA was proposed in 2012 by X.S. Yang and uses the flower pollination process (Yang, 2012; Yang et al., 2013). FPA follow the 4 rule, which are expressed as:

- Biotic/cross-pollination, is considered as global pollination process with pollens following Lévy flights
- Self-pollination/abiotic pollination, helps in local pollination.
- Pollinators can develop flower constancy (reproduction probability), and is proportional to the similarity index of the two flowers involved.
- Local and global pollination is regulated by switch probability $\in$ [0, 1].

In FPA, a pollen particle's location is represented by the solution vector a_i (rule 1), presented in Eq. (20).

$$a_i^{t+1} = a_i^t + L(\lambda)(a_i^t - g_*) \tag{20}$$

Where, pollen (a_i^t), current best solution (g_*), and pollination strength (L). Since insects sometimes fly over large distances in many distance steps, we may effectively simulate this behaviour using a Lévy flight. Specifically, take $L > 0$ from a Lévy distribution is given in Eq. (21).

$$L(\lambda) \sim \frac{\lambda\Gamma(\lambda)\sin(\pi\lambda/2)}{\pi}\quad \frac{1}{s^{1+\lambda}}\quad (s \gg s_0 \gg 0) \tag{21}$$

Then, both Rule 2 and Rule 3 can be expressed in Eq. (22) to describe the local pollination.

$$a_i^{t+1} = a_i^t + \varepsilon(a_j^t - a_k^t) \tag{22}$$

where standard gamma function ($\Gamma(\lambda)$), pollen from several flowers of the same type of plant ($a_j^t and a_k^t$), uniform distribution ($\varepsilon = [0, 1]$).

Even though pollination takes place both locally and globally, it is more likely that nearby flowers are pollinated. To simulate this, using a switch probability (p) with an initial value of $p = 0.5$ is considered.

3.2. Grey wolf optimization

GWO algorithm is based on the foraging of grey wolves found in nature. These animals live in groups, and the population in each group is separated into four categories. The first category is the alpha group, then followed by beta, delta and Omega wolves occupied the lowest category. Alpha wolves are also known as dominating wolves because their orders are followed by the entire group. The following are the primary stages of grey wolf group hunting: encircling; hunting; and attacking (Mirjalili et al., 2014b).

3.2.1. Social hierarchy

The grey wolves' social hierarchy must be simulated when implementing the GWO algorithm. The fittest solution among the whole population is considered alpha (α) in each iteration, followed by beta (β), delta (δ), and remaining are omega (ω). The ω-hunting wolves follow these α, β, and δ in the GWO algorithm.

3.2.2. Encircling prey

Encircling the prey is the initial stage of the hunting process. To mathematically describe the encircling behaviour can be expressed in Eqs. (23), and (24):

$$\vec{E} = \left|\vec{F}.\vec{Y}_p(t) - \vec{Y}(t)\right| \tag{23}$$

$$\vec{Y}(t+1) = \vec{Y}_p(t) - \vec{B}.\vec{E} \tag{24}$$

where, $\vec{B}$ and $\vec{F}$ are the coefficient vectors, t is the present iteration, $\vec{X}_p$ is position vector of prey, and position vector of a grey wolf($\vec{X}$).

The $\vec{B}$ and $\vec{F}$ are presented in the Eqs. (25), and (26).

$$\vec{B} = 2\vec{a}.\vec{r}_1 - \vec{a} \tag{25}$$

$$\vec{F} = 2.\vec{r}_2 \tag{26}$$

where, $\vec{a}$ are linearly decreased [2–0], and random vector (r_1, r_2 = [0, 1])

3.2.3. Hunting

The top three fittest individuals of the grey wolf population, α, β, and δ are well-versed in the location of prey. Hence the location of the ω are changed with respect to the α, β, and δ. The following Eqs. (27) to (29) are utilized in this regard.

$$\vec{D}_\alpha = \left|\vec{C}_1.\vec{Y}_\alpha - \vec{Y}\right|; \vec{D}_\beta = \left|\vec{C}_2.\vec{Y}_\beta - \vec{Y}\right|; \vec{D}_\delta = \left|\vec{C}_3.\vec{Y}_\delta - \vec{Y}\right| \tag{27}$$

$$\vec{Y}_1 = \vec{Y}_\alpha - \vec{B}_1.(\vec{E}_\alpha); \vec{Y}_2 = \vec{Y}_\beta - \vec{B}_2.(\vec{E}_\beta); \vec{Y}_3 = \vec{Y}_\delta - \vec{B}_3.(\vec{E}_\delta) \tag{28}$$

$$\vec{Y}(t+1) = \frac{\vec{Y}_1 + \vec{Y}_2 + \vec{Y}_3}{3} \tag{29}$$

3.2.4. Attacking prey

During the hunting process, the value of $\vec{a}$ falls from 2 to 0, and so the value of $\vec{B}$ decreases, as seen in Eq. (25). When the value of $\vec{B}$ is between [−1, 1], the step size given is quite small, and the agent's next location is very near to the prey's location. It indicates that wolves in this region of $\vec{B}$ travel in the towards of the prey.

3.2.5. Search for prey

Grey wolves mainly use the α, β, and δ locations to guide their search. Grey wolves separate from one another and join to attack the prey in order to find a new solution (prey), and this is achieved in the GWO by the utilization of parameter $\vec{B}$. The new location of the search agents will be far from the prey if the value of $\vec{B}$ is less than or equal to 1 and produces a large value of step size. Another parameter $\vec{F}$, controls the *expl* of search agents and prevents stagnation in local optima by giving the prey random weight, which increases the prey's impact on $\vec{F} > 1$ while decreasing the impact of the prey on $\vec{F} < 1$.

Grey wolves population is initialized in the beginning. The top three fittest individuals (α, β, and δ) are selected for each iteration to guide the other wolves to the location of the prey. The value of $\vec{a}$ is linearly reduced from 2 to 0 during the hunting process, which results in a decrease in the range of $\vec{B}$. When $\vec{B} < 1$ occurs, the search space is exploited; when $\vec{B} > 1$ occurs, the algorithm's *expl* is enhanced.

3.3. Differential evolution

DE algorithm is based on Darwin's theory of evolution (Storn, 1995). The fundamental DE algorithmic framework is divided into four steps (Ahmad et al., 2022; Pant et al., 2020):

3.3.1. Initialization

During the phase of initialization, a set of populations with a uniform distribution is generated in the following Eq. (30):

$$Y_j^G = Y_{lb} + (Y_{ub} - Y_{lb}) * rand(0,1) \tag{30}$$

where, upper and lower boundary ($Y_{ub}, and Y_{lb}$), and random number ($rand = (0,1)$)

3.3.2. Mutation

During the process of mutation, a mutant vector W_j^G is produced for each target vector Y_{r1}^G at generation G, can be expressed in Eq. (31) .

$$W_j^G = Y_{r1}^G + H * (Y_{r2}^G - Y_{r3}^G) \tag{31}$$

where scaling factor ($F = [1,0]$), mutually different, randomly chosen vectors ($r1$, $r2$, $r3 \in 1,2, \ldots$.NP)

3.3.3. Crossover

After mutation, a crossover is performed in order to generate the trial vector, which is represented in the following Eq. (32).

$$T_j^G = \left\{ t_{1,j}^G, t_{2,j}^G, t_{3,j}^G \ldots\ldots\ldots\ldots, t_{D,j}^G \right\} \tag{32}$$

The process of crossover is carried out and is given by Eq. (33).

$$Y_j^G = \left\{ y_{1,j}^G, y_{2,j}^G, y_{3,j}^G, \ldots \ldots\ldots\ldots, y_{D,j}^G \right\} \tag{33}$$

The mutant vector W_j^G using a crossover probability C_r whose value is between 01. T_j^G is given in Eq. (34).

$$t_{i,j}^G = \begin{cases} w_{i,j}^G if randj \le C_r \\ y_{i,j}^G, otherwise \end{cases} \tag{34}$$

where, i ∈ 1,2,3.....,D

3.3.4. Selection

After formulating the solutions, the best solution from the previous and the current iteration is selected. The following is a mathematical representation of the procedure that DE uses to select candidates is presented in Eq. (35):

$$Y_j^{G+1} = \begin{cases} T_j^G, if, f(T_j^G) \le f(Y_j^G) \\ Y_j^G otherwise \end{cases} \tag{35}$$

4. The proposed HFGD algorithm

FPA has already established its significance over various domain research problems. This algorithm has good *expl* and *expt* properties but for a highly complex optimization problem, it becomes really very challenging to solve problems using basic FPA. Also, the algorithm has poor *expl*, and also lacks a proper balance between the global search and the local search. The algorithm also is computationally expensive, and new modifications must be added to make it best fit for all optimization problems. Keeping these points in mind, a hybrid algorithm based on three algorithms is proposed. The three algorithms used include FPA (Yang, 2012), GWO (Mirjalili et al., 2014b) and DE (Storn, 1995) and is named as Hybrid Flower Grey Differential (HFGD) algorithm. New concepts of division of generation, and adaptive parametric settings are also introduced to propose the new algorithm. Changes have been incorporated in the local and global search phase to improve the *expl* and *expt* properties. Apart from that, population adaptation is added to decrease the total function evaluations and improve the computational complexity. Adaptive parametric settings are also added to make the algorithm self-adaptive and self-sufficient in operation.

4.1. Why each modification is added

This proposal adds four new modifications to the basic structure of FPA. The need for these modifications is discussed in this subsection. The basic modifications added include iterative division, the introduction of bare-bones mechanism, adaptive parameters, and population adaptation. The first and foremost modification is the adaption of division of generations. By iterative division, we mean that, multiple sets of generations are used for both global and local search operation. We use two different set of generations, and each set use a different equation for evaluating new solutions. The process is employed such that for the first iterative half, higher *expl* and lesser *expt* is followed, whereas for the other iterative half, equations that help in higher *expt* and lower *expl* is employed. During the first half of iterations, the global search is controlled by using FPA based equations, which help the algorithm in *expl* potential areas of the search space. Local search during this half is controlled by using a sinusoidal frequency component in the local search equations of FPA, and is meant for providing intensive exploitation. In the second half of the iterations, the *expl* should decrease and *expt* must increase. GWO based equations have been found to provide such properties (Salgotra et al., 2020b). Here we are using a modified equation based on the GWO characteristics for the global search phase. For the local search phase in the second iterative half, DE based equations are added. These equations are meant to provide extensive exploitative tendencies, which are achieved by using this equation in combination with simulated annealing based mutation operators (Salgotra et al., 2021b).

The second modification is the addition of a bare-bones mechanism. This mechanism is not new and has been exploited in recent times in some of the major algorithms including DE, PSO and others. By adding a bare-bones mechanism, we find that the working properties of the algorithm improve significantly. This component has enhanced initial *expl* due to larger step sizes, whereas with the progression of iterations, the standard deviation approaches zero, resulting in increased *expt* towards the end. Thus helping in *expl* as well as *expt* simultaneously, and further reducing local optima stagnation.

Overall, there are two parameters in the proposed algorithm, known as switch probability (p_a), which helps in switching from *expl* to *expt* and vice versa. Most of the algorithms perform well on unimodal and multimodal functions, but as the complexity of the problem increases, the total number of local minima also increase many folds and this can be achieved by designing a balanced *expl* and *expt* phase. Hence, there is a requirement of better set of parameters. A normal p_a is calculated in the range of $[0,1]$, but significant studies have shown that adaptive switching provides better results. A larger value of p_a

implies better *expl*, whereas smaller values correspond to more *expt*. A value of $p_a = 1$ means 100% *expl* and $p_a = 0$ means 100% *expt*. Thus, a gradual shift from 1 to 0 will make the algorithm move from *expl* to *expt* over subsequent iterations. For a gradual decrease, we use simulated annealing-based parameter adaptation. This parametric distribution makes the algorithm follow extensive *expl* during the initial stages and intensive *expt* in the end, hence helping in a balanced approach.

All the algorithms use a predefined set of initial parameters, and population size is one among those. Higher population sizes are required for more *expl*, whereas lower population sizes help in better *expt*. In order to achieve this, population adaption is an important characteristic followed recently in evolutionary algorithms. A constantly reducing population size helps to exploit this property and hence aims at achieving better solution quality. We use a proportional population size reduction mechanism to adaptively reduce the population size over subsequent iterations. This helps the algorithm in reducing the total number of function evaluations. More details about the proposal are presented below.

4.2. The proposal

The proposed algorithm follows the basic structure of initialization, global search phase, local search phase and finally the selection operation. The new algorithm also follows division of generations to make the algorithm more efficient in terms of *expl* and *expt*. Detailed modifications and the reason for the addition of these modifications are presented below.

Initialization: A general initialization phase follows a random population of N, distributed randomly with in lower bounds $N_{min,j}$ and upper bounds $N_{max,j}$, for a certain variable size of D, and is given by Eq. (36):

$$N_{i,j} = N_{min,j} + R(0,1) \times (N_{min,j} - N_{max,j}) \tag{36}$$

where $i \in [1,2,\ldots,N]$, $j \in [1,2,\ldots,D]$, $N_{i,j}$ is the solution for jth D, $R(0,1) \in [0,1]$. The next step is the global and local search phase, which in the current scenario is divided into two set of generations.

Phase I: *for generation* $\leq$ $maximumgenerations/2$ During the first half of generations, the global search phase is followed by the basic equations of flower pollination algorithm with the addition of modified bare-bones generalization inspired by self-adaptive cuckoo search algorithms (Salgotra et al., 2021a). The basic equations are given in Eqs. (37) and (38).

$$p_i^{t+1} = p_i^t + \alpha \otimes L(\lambda)(p_{best} - p_i^t) \tag{37}$$

$$L(\lambda) \sim \frac{\lambda \Gamma(\lambda) \sin(\pi\lambda/2)}{\pi} \quad \frac{1}{s^{1+\lambda}} \quad (s \gg s_0 \gg 0) \tag{38}$$

The Eqs. (39) inspired by barebones is given as:

$$gp_{i,D} = R_w \times p_{new}^{t+1} + (1 - R_w) \times bp_{i,D} \tag{39}$$

for $bp_{i,D} = N(\frac{p_{j,D}^t + p_{k,D}^t}{2}, |s_{j,D}^t - p_{k,D}^t|)$ where $gp_{i,D}$ is the new solution generated in global search, D and $R_w \in [0,1]$ is a random weight coefficient; x_{best} is the best, p_j^t and p_k^t are two random solutions in the tth iteration respectively. The concept of barebones is a cooperative search mechanism and is added for diversity in the solution quality. The mechanism has already been used in some recently proposed algorithms, and it improves the overall *expl* during the global search phase. During the initial stages, this mechanism generates large step sizes and starts moving towards the global minima towards the later stages. This makes the HFGD algorithm follow both *expl* and *expt* simultaneously.

The next phase is the local search, and the general equations in this phase is given in Eq. (40)

$$p_i^{t+1} = p_i^t + \alpha \times H(p_a - \epsilon) \times (p_j^t - p_k^t) \tag{40}$$

where p_i^t is the previous solution, $\epsilon \in [0,1]$, p_a is the probability to control *expl* versus the *expt*. The ϵ parameter is modified using a f_{req} sinusoidal function of fixed frequency and is presented in Eq. (41).

$$F_i^{t+1} = \frac{1}{2} \times (sin(2\pi \times f_{req} \times t + \pi) \times \frac{t_{max-t}}{t_{max}} + 1); \; if \; r_1 > 0.5 \tag{41}$$

$$F_i^{t+1} = \frac{1}{2} \times (sin(2\pi \times f_{req} \times t) \times \frac{t_{max-t}}{t_{max}} + 1); \; if \; r_1 < 0.5 \tag{42}$$

Here t and t_{max} respectively denote the current and maximum iterations. Note that this phase is meant to improve the *expl* operation and hence less effort are paid to improve the *expt* operation.

Phase II: *for generation* $\geq$ $maximumgenerations/2$*:* During the second half of generations, *expt* operation is made more prevalent by adding GWO-inspired modifications. These equations are inspired by the self-adaptive multi-hybrid algorithm (MHA) (Salgotra et al., 2021b). The generalized equations are given in Eq. (43)

$$\begin{cases} w_1 = p_i - M_1(R_1.p_{new} - p_i^t); \\ w_2 = p_i - M_2(R_2.p_{new} - p_i^t); \\ w_3 = p_i - M_3(R_3.p_{new} - p_i^t); \\ p_i^{t+1} = \frac{w_1 + w_2 + w_3}{3} \end{cases} \tag{43}$$

Here p_{new} is the new solution and M_1, M_2, M_3 and R_1, R_2, R_3 corresponds to M and R respectively. The variables M and Q are defined in Eq. (44)

$$\begin{cases} M = 2a.r_1 - a; \\ R = 2.r_2 \end{cases} \tag{44}$$

where a is linearly decreasing from $[2,0]$ iteratively, r_1 and r_2 are $\in [0,1]$. The priority is to find solutions close to the search agents and hence contribute towards the local search operation. This is followed to exploit potentially towards the end.

Local search during this phase is governed by using equations of the DE algorithm. These equations are meant for extensive *expt* operation and the generalized equation is given in Eq. (45).

$$p_i^{t+1} = (1 - \lambda)p_i^t + \lambda(p_{best} - p_i^t) \tag{45}$$

where p_i^t and p_i^{t+1} defines the ith solution for current t_th and λ is the scaling factor. In the current case, λ is inspired from simulated annealing mutation operator (Salgotra et al., 2021b) and is given in Eq. (46).

$$\lambda = \gamma_{min} + (\gamma_{max} - \gamma_{min}) \times b^{(k-1)} \tag{46}$$

where γ_{min}=0.5, γ_{max}=0.9, $k \in$ [0,1] and value of b is set to 0.95.

Selection Operation The next step is meant for selecting a current best solution in comparison to the previous best solution. A generalized selection operation is given in Eq. (47).

$$p_{new}^{t+1} = \begin{cases} p_{new} & if \; f(p_{new}) < f(p_i^t) \\ p_i^t & otherwise \end{cases} \tag{47}$$

where p_{new} is the new solution found after selection.

Population adaptation is followed with a larger population size for enhanced *expl* and reducing it to a lower population size for *expt*. A major thing to keep in mind is the best solution must not be lost in the process for effective operation. Various different population adaptation policies have been exploited in the literature (Salgotra et al., 2020a) but it has been found that one of the best strategies is the shrinking adaptation. Here, better genetic drift is found using smaller population sizes, and the best solution is kept as such. This strategy is significantly important if there is only a small variation in solution quality, and in such a case using a smaller population size is economical. The general equation is given in Eq. (48).

$$Q_{t+1} = \begin{cases} (1 - \Delta g_t^{best})Q_t, & if \Delta g_t^{best} \leq \Delta f_{max}^{best} \\ (1 - \Delta f_{max}^{best})Q_t, & if \Delta g_t^{best} > \Delta f_{max}^{best} \\ min_N, & if Q_{t+1} < min_N \end{cases} \tag{48}$$

Q_{t+1} is the population size at t_{th} generation t, Δg_t^{best} is given by $(\frac{f_{t-1}^{best} - f_{t-2}^{best}}{|f_{t-2}^{best}|})$ is the change in the best fitness, Δf_{max}^{best} is the threshold value.

Apart from that, the computation complexity of an algorithm is directly given by: "population size multiplied by the total number of iterations". For a fixed number of iteration, if the population size is very high, computational complexity will increase many folds. Whereas when the population size keeps on reducing over subsequent iterations, the total number of function evaluation will automatically reduce and hence the computation burden will be less low. Thus, a reducing population adaptation helps in reducing the Computational burden substantially.

The pseudocode for the proposed HFGD algorithm is given in 1.

Algorithm 1 Pseudocode of HFGD algorithm

```
Begin
Define: population size (N);
        stopping criteria; problem dimension (D)
if i= 1: maximum generations / 2 then
    global search using Eqn. (37)
    local search using Eqn. (40)
    evaluate fitness
    perform greedy selection using Eqn. (47)
    Update population size using Eqn. (48)
else
    global search using Eqn. (45)
    local search using Eqn. (43)
    evaluate fitness
    perform greedy selection using Eqn. (47)
    Update population size using Eqn. (48)
    close;
update final best
End
```

5. Experimental results

Here, the effectiveness of the HFGD algorithm is validated by using well known benchmark numerical test problems (CEC 2019) and extracting the optimal PV parameters. In this paper, first, the effectiveness and robustness of the HFGD is tested with the benchmark numerical test problems (CEC 2019) and compared with serval MH optimization algorithms. Then the HFGD algorithm is tested for four classical PV parameters estimation challenges (SDM, DDM, Amorphous Silicon aSi:H, and PVM 752 GaAs Thin-Film), and the outcomes of the HFGD algorithm are compared with other MH algorithms. The outcomes shows that the proposed HFGD algorithm can effectively handle the challenges mentioned above and outperform the rest of the MH algorithms. The proposed HFGD algorithm and other comparative MH algorithms are implemented in this research using the MATLAB R2022b software on a Windows 11 operating system, 64-bit operating system, x64-based Intel(R) CPU, i5 12500H (2.50 GHz) processor, and 16 GB of RAM.

5.1. Benchmark numerical test problems (CEC 2019)

This section gives statistical results of the proposed HFGD and its comparison with jDE100 (Brest et al., 2019), FPA (Yang, 2012), YDSE (Abdel-Basset et al., 2023) and others, using most complex 100-digit problem (CEC 2019) numerical challenges. Table 2 compares the performance of the proposed HFGD algorithm to that of well-known algorithms such as DE (Storn and Price, 1997), jDE100 (Brest et al., 2019), FPA (Yang, 2012), GWO (Mirjalili et al., 2014a), PSO (Wu et al., 2022), EWOA (Reddy and Saha, 2022) and YDSE (Abdel-Basset et al., 2023). Table 1 tabulated the parametric setting of all compared MH algorithms on the Benchmark numerical test problems (CEC 2019). All parameters for the algorithms under test are kept the same, and the simulated results are reported in terms of the mean and standard deviation for 51 simulations of each algorithm with 500 iterations and a population size of 50.

Table 2's results demonstrate that EWOA can outperform other algorithms while solving np_1, and np_6, and np_1 challenge, but HFGD algorithm is proven to be superior to the alternatives. According to the simulation results shown in Table 2, HFGD algorithm outperforms competing algorithms for solving numerical problems np_2, np_4, np_5, np_7, np_9 and np_{10} in terms of the mean value. For challenge np_3, EWOA, and HFGD algorithms shows best outcomes as compared to the other MH algorithms. Finally, the working efficiency of the GWO is best for challenge np_8. Thus, the HFGD algorithm is effective for eight out of ten numerical test problems, whereas jDE100, and GWO are effective for one problem.

In addition, the Friedman (f-rank) test and rank-sum (p-rank) test are used to assess HFGD algorithm efficiency. First, the analysis is performed in terms of win(w), loss (l), and tie (t) to calculate p-rank. Initially, when the comparative optimization approach surpasses the HFGD algorithm, the circumstance is represented with a "+" and referred to as a "win(w)" situation. The "−" symbol is used because the performance of the test method in the loss (l) scenario is inferior to that of the HFGD algorithm. In the event of a tie (t), the "=" signifies that the competing algorithms are equally capable. As illustrated in the third row of each numerical problem, the recommended optimization strategy, HFGD algorithm, outperforms in the majority of situations.jDE100, FPA, and YDSE win the proposed HFGD algorithm for one challenge (np_1). And also, GWO win the proposed HFGD algorithm for two challenge (np_1, and np_8). Second, the f-rank test assigns a unique f-rank to each algorithm under consideration. Based on the second last and last row of Table 2, the F-rank is computed, and it is determined that the proposed HFGD algorithm has got Ist rank. In addition to statistical results, the convergence profiles of YDSE, GWO, and DE, and the proposed HFGD algorithm are presented for 5 numerical problems (np_2, np_5, np_6, np_8, as well as np_{10}) in Fig. 4. According to the plot, the HFGD algorithm converges faster than YDSE, GWO, and DE for all numerical problems (np_2, np_5, np_6, and np_{10}) considered. The HFGD algorithm consistently has a greater convergence rate than YDSE, GWO, and DE algorithms.

5.2. Results and discussion on the PV

To further validate the optimization capability, the HFGD algorithm are utilized to calculate the optimal parameter of SDM, DDM, Amorphous Silicon aSi:H, and PVM 752 GaAs Thin-Film solar PV modules/cells. The main aim is to estimate the five parameters (R_s, N, I_{sc}, R_{shu}, and I_{Ph}) of the SDM, Amorphous Silicon aSi:H, and PVM 752 GaAs Thin-Film and seven parameters (R_s, N_1 and N_2, I_{sc1}, I_{sc2}, R_{shu}, and I_{Ph}) for DDM. The obtained simulation findings using the proposed HFGD algorithm are compared to the most recently published MH algorithms reported in the literature. Furthermore, statistical analysis is performed by evaluating $IAE_{current}$, IAE_{power}, RE, MBE, MAE, and MAPE values to determine the quality of the curve fit between HFGD parameters and the experimental data. The $IAE_{current}$, IAE_{power}, RE, MBE, MAE, and MAPE values are calculated by using the above-mentioned Eqs. (10), (11) (12), (13), (14) and (15), respectively. Also, the Friedman and Wilcoxon tests are carried out to validate the robustness and accuracy of the proposed HFGD algorithm.

The proposed HFGD algorithm are implemented in this research using the MATLAB R2022b software on a Windows 11 operating system, 64-bit operating system, x64-based Intel(R) CPU, i5 12500H (2.50 GHz) processor, and 16 GB of RAM. The simulation studies utilized a population size of 70 and 30 run for HFGD algorithm. The upper (UB) and lower boundary (LB) limits are tabulated in Table 3 and are the same as reported in other literatures (Li et al., 2019a; Ali et al., 2023).

Table 1
Parametric details of different algorithms for CEC 2019.

Algorithm	Parameters
FPA (Yang, 2012)	λ=1.5; ε = [0,1], $p = 0.5$
GWO (Mirjalili et al., 2014a)	$\vec{\alpha}$ = Linearly decreasing [2,0]
JDE 100 (Brest et al., 2019)	$\tau_1 = 0.1$; $\tau_2 = 0.1$, $CR_{init} = 0.5$; $F_{init} = 0.5$; $CR_u = 1.1$; $F_u = 1.1$, $CR_l = [0.1, 1.0]$
YDSE (Abdel-Basset et al., 2023)	$\lambda = 5X10^{-06}$; $d = 5X10^{-03}$; $I = 0.01$
DE (Abd Elaziz et al., 2020)	$F = 0.5$; $CR = 0.9$
HFGD	$b = 0.95$; α = Linearly decreasing [2,0]; r_1, r_2 = [0,1]; $\gamma_{min} = 0.5$; $\gamma_{max} = 0.9$,

Table 2
100-digit challenge for numerical (CEC 2019) problems.

Problem		HFGD	DE (Storn and Price, 1997)	jDE100 (Brest et al., 2019)	FPA (Yang, 2012)	YDSE (Abdel-Basset et al., 2023)	GWO (Mirjalili et al., 2014a)	PSO (Wu et al., 2022)	EWOA (Reddy and Saha, 2022)
np_1	Mean	1.000E+10	5.864E+11	**1.590E+05**	5.41E+08	1.836E+06	1.146E+08	2.2371E+10	6.794E+04
	Std	**0.000E+00**	8.359E+11	1.597E+05	2.939E+08	9.262E+05	2.387E+08	1.7275E+10	1.252E+04
	p-rank		−	+	+	+	+	−	+
	f-rank	6	8	2	5	1	4	7	1
np_2	Mean	**1.734E+01**	6.844E+01	2.163E+01	2.385E+06	**1.735E+01**	1.749E+01	2.7232E+01	1.736E+01
	Std	1.041E−04	1.418E+02	2.719E+04	2.6141E+00	**4.300E−03**	2.231E−04	5.3829E+01	4.2862E−02
	p-rank		−	−	−	−	−	−	−
	f-rank	1	7	6	8	2	4	5	3
np_3	Mean	**1.270E+01**	**1.270E+01**	1.310E+06	**1.270E+01**	**1.270E+01**	**1.270E+01**	**1.270E+01**	**1.270E+01**
	Std	**2.208E−14**	1.900E−03	8.519E+05	9.0311E−08	3.494E−05	2.139E−07	7.5574E−04	0.000E+00
	p-rank		−	−	−	−	−	−	+
	f-rank	2	7	8	3	5	4	6	1
np_4	Mean	**3.898E+01**	1.539E+03	3.475E+05	1.343E+02	5.389E+01	9.2957E+01	1.2030E+03	1.559E+02
	Std	**6.937E+00**	2.433E+03	1.149E+05	2.805E+01	1.037E+01	2.190E+02	6.6790E+02	6.482E+01
	p-rank		−	−	−		−	−	−
	f-rank	1	7	8	4	2	3	6	5
np_5	Mean	**1.1513E+00**	2.116E+00	1.673E+05	1.6368E+00	2.170E+00	1.408E+00	1.6473E+00	8.132E+00
	Std	**3.263E−04**	2.850E−01	8.426E+04	8.526E−02	6.468E−01	2.576E−01	4.3138E−01	0.000E+00
	p-rank		−	−	−	−	−	−	−
	f-rank	1	5	8	3	6	2	4	7
np_6	Mean	9.716E+00	9.901E+00	3.841E+04	1.049E+01	1.007E+01	1.081E+01	8.5524E+00	**7.924E+00**
	Std	7.416E−01	1.474E+00	2.063E+03	6.747E−01	6.818E−01	6.673E−01	1.1533E+00	1.286E+00
	p-rank		−	−	−	−	−	+	+
	f-rank	3	4	8	7	5	6	2	1
np_7	Mean	**6.315E+01**	1.282E+03	9.105E+06	2.662E+02	2.658E+02	3.474E+02	3.2512E+02	2.097E+03
	Std	**5.941E+01**	4.224E+02	4.38E+08	1.025E+02	1.193E+02	2.886E+02	2.8856E+02	0.000E+00
	p-rank		−	−	−	−	−	−	−
	f-rank	1	6	8	4	5	3	2	7
np_8	Mean	5.322E+00	6.982E+00	1.219E+09	5.836E+00	6.007E+00	**4.699E+00**	5.4877E+00	7.879E+00
	Std	3.845E−01	2.255E−01	4.388E+08	2.7187E−01	3.456E−01	**1.219E+00**	6.8809E−01	0.000E+00
	p-rank		−	−	−	−	+	−	−
	f-rank	2	6	8	4	5	1	3	7
np_9	Mean	**2.680E+00**	2.788E+02	9.207E+08	4.947E+00	6.172E+01	4.250E+00	3.4069E+01	4.710E+03
	Std	**1.379E−01**	3.122E+02	1.131E+08	4.190E−01	1.523E+02	9.427E−01	4.0954E+01	0.000E+00
	p-rank		−	−	−	−	−	−	−
	f-rank	1	6	8	3	5	2	4	7
np_{10}	Mean	**1.994E+01**	2.042E+01	1.541E+06	2.039E+01	2.039E+01	2.0434E+01	2.0041E+01	2.090E+01
	Std	2.440E+00	1.295E−01	7.460E+05	7.951E−02	1.034E−01	1.025E−01	5.4341E−02	1.631E−03
	p-rank		−	−	−	−	−	−	−
	f-rank	1	6	8	3	4	5	2	7
w/l/t		NA	0/10/0	1/9/0	1/9/0	1/9/0	2/8/0	1/9/0	3/7/0
Average f-rank		1.90	6.20	7.20	4.40	4.00	3.40	4.10	4.60
Overall f-rank		1	7	8	5	3	2	4	6

Table 3
Parameters limits for SDM, DDM, Amorphous Silicon aSi:H, and PVM 752 GaAs Thin-Film.

Parameters	SDM		DDM		Amorphous Silicon aSi:H		PVM 752 GaAs	
	LB	UB	LB	UB	LB	UB	LB	UB
N/N1, N2	1	2	1	2	1	5	1	2
Rshunt or Rsh (Ω)	0	100	0	100	0	1000	0	1000
Rs (Ω)	0	0.5	0	0.5	0	0.5	0	1
I_{sc1} / I_{sc2} *or* I_{o1}/I_{o2} (μA)	0	1	0	1	0	10	0	1
I_{Ph} (A)	0	1	0	1	0	0.1	0	1

5.2.1. Parameter extraction of RTC. France solar cell (SDM)

The RTC France solar PV cell data-sheet is extracted from (Düzenli et al., 2022), which is extensively mentioned in published papers of literature. For the SDM, the IAE and RE between the measured as well as estimated data are tabulated in Table 4. And also, Table 4 presents the $IAE_{current}$, IAE_{power}, MAE, MBE, SSE, RMSE, MAPE, MBE, NMAE, NMBE, NRMSE, and Im values. The $IAE_{current}$ and IAE_{power} values are 0.017632 and 0.006481. Table 5 shows the comparison outcomes, including IAE, RMSE (minimum (min), mean and standard deviation (Std.)), and five unknown parameters (R_s, N, I_{sc}, R_{shu}, and I_{Ph}) values. The algorithms with the lowest RMSE values are displayed in boldface. The HFGD algorithm offers the least RMSE value (7.72E−04), which can validate the accuracy of the HFGD algorithm. To further demonstrate the quality of the obtained outcomes, the best HFGD algorithm parameters are utilized to reconstruct the I–V and P–V curves seen in Figs. 5(a) and 5(b). As seen in Figs. 5(a) and 5(b), the computed outcomes by HFGD algorithm are in excellent agreement with the available data over the entire voltage range.

5.2.2. Parameter extraction of RTC. France solar cell (double diode model)

The HFGD algorithm is employed to extract the solar PV characteristics for a DDM of 57 mm diameter commercial (RTC France) silicon solar cells under specific conditions, namely a temperature of 33 °C and an irradiation of 1000 W/m^2. The data sheet for the RTC France

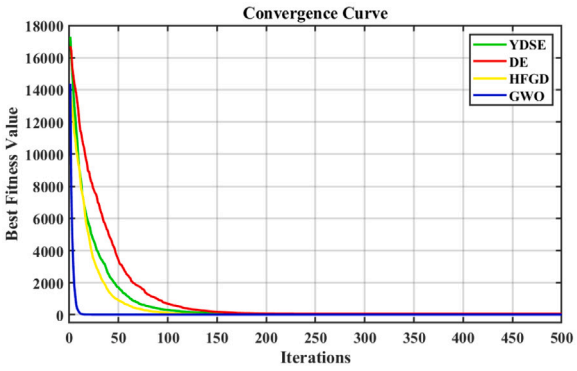

(a) Convergence profile (np_2)

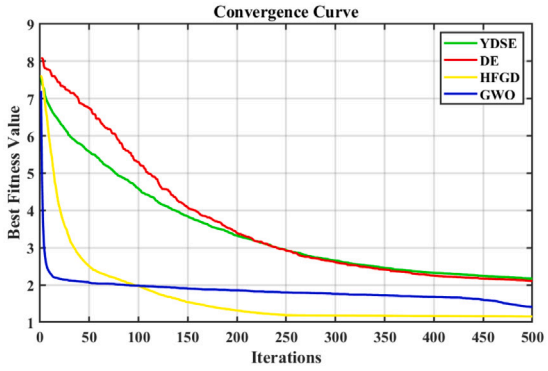

(b) Convergence profile (np_5)

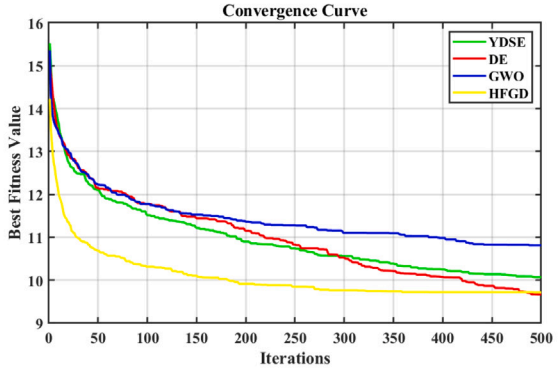

(c) Convergence profile (np_6)

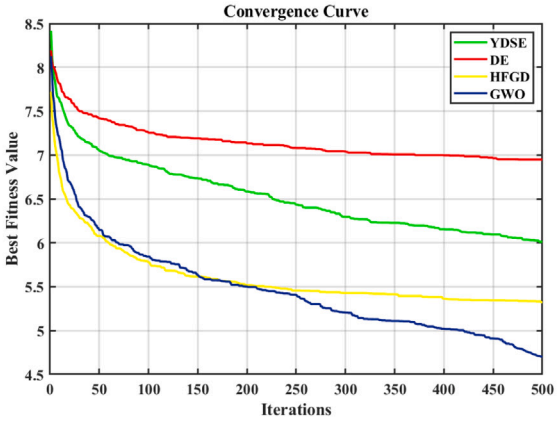

(d) Convergence profile (np_8)

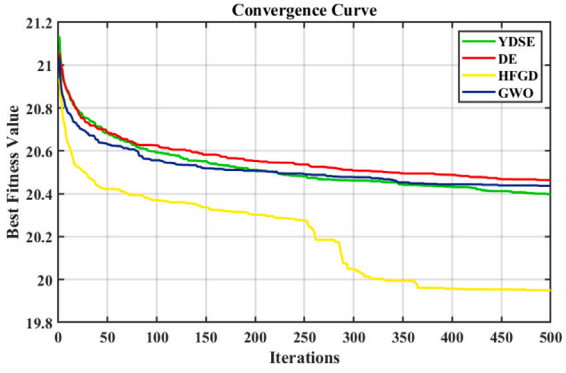

(e) Convergence profile (np_{10})

Fig. 4. Convergence profiles of YDSE, DE, HFGD and GWO for numerical (CEC 2019) problems.

solar PV cell, which has been widely utilized in relevant literature, has been obtained from Düzenli et al. (2022). For the DDM, Table 6 presents the $IAE_{current}$, IAE_{power}, SSE, RMSE, MAPE, MBE, NMAE, NMBE, NRMSE, Im, and RE values. The best $IAE_{current}$, and IAE_{power}, values are 0.017067785 and 0.006445256. Table 7 shows the comparison outcomes, including IAE, RMSE, and seven unknown parameters (I_{Ph}, I_{sc1}, I_{sc2} R_{shu}, R_s, $N1$ and $N2$). The HFGD algorithm clearly provides the lowest RMSE value (7.48E−04), which can validate the accuracy. The algorithms with the lowest RMSE values are displayed in boldface. The I–V and P–V curves of the simulated data obtained by HFGD optimization technique are remarkably compatible with the experimental data, as shown in Figs. 6(a) and 6(b).

5.2.3. Parameter extraction of Amorphous Silicon aSi:H

The HFGD algorithm is utilized to extract the solar PV characteristics for a Amorphous Silicon aSi:H of 1 cm^2 area under specific conditions, namely a temperature of 25 °C and an irradiation of 1000 W/m^2, including a total of 46 I–V measured data. The data sheet for the Amorphous Silicon aSi:H solar PV cell, which has been widely utilized in relevant literature, has been obtained from Cotfas et al. (2021). The best $IAE_{current}$, as well as IAE_{power}, SSE, RMSE, MAPE, MBE, NMAE, NMBE, NRMSE, and Im of Amorphous Silicon aSi:H, are tabulated in Table 8. The best $IAE_{current}$, and IAE_{power}, values are 0.001812 and 0.000818. The outcomes of the HFGD algorithm are compared with the recent MH algorithm. The HFGD algorithm gives the best objective function value (RMSE) is 4.61E−05. The optimal parameters as well as $IAE_{current}$, mean, min and std value of the objective function are presented in Table 9. The robustness and accuracy of the HFGD algorithm are reflected by well-known I–V, and P–V curves of the PV module are presented in Figs. 7(a) and 7(b).

Table 4
The HFGD outcomes of Ie, IAE, MAE, MBE, MAPE, SSE, NMAE, NMBE, NRMSE, and RE for the RTC SDM.

S.No	Ie	Im	IAE	V	Pe	Pm	IAE	RE
1	0.764149	0.764	0.000149	−0.2057	−0.15719	−0.15715	3.07E−05	−0.0002
2	0.762702	0.762	0.000702	−0.1291	−0.09846	−0.09837	9.06E−05	−0.00092
3	0.761374	0.7605	0.000874	−0.0588	−0.04477	−0.04472	5.14E−05	−0.00115
4	0.760155	0.7605	0.000345	0.0057	0.004333	0.004335	1.97E−06	0.000454
5	0.759039	0.76	0.000961	0.0646	0.049034	0.049096	6.21E−05	0.001264
6	0.758011	0.759	0.000989	0.1185	0.089824	0.089942	0.000117	0.001303
7	0.757046	0.757	4.57E−05	0.1678	0.127032	0.127025	7.67E−06	−6E−05
8	0.756085	0.757	0.000915	0.2132	0.161197	0.161392	0.000195	0.001209
9	0.755022	0.7555	0.000478	0.2545	0.192153	0.192275	0.000122	0.000632
10	0.753597	0.754	0.000403	0.2924	0.220352	0.22047	0.000118	0.000534
11	0.751327	0.7505	0.000827	0.3269	0.245609	0.245338	0.00027	−0.0011
12	0.747305	0.7465	0.000805	0.3585	0.267909	0.26762	0.000289	−0.00108
13	0.740085	0.7385	0.001585	0.3873	0.286635	0.286021	0.000614	−0.00215
14	0.727426	0.728	0.000574	0.4137	0.300936	0.301174	0.000237	0.000788
15	0.707026	0.7065	0.000526	0.4373	0.309182	0.308952	0.00023	−0.00074
16	0.6754	0.6755	9.97E−05	0.459	0.310009	0.310055	4.58E−05	0.000148
17	0.630998	0.632	0.001002	0.4784	0.30187	0.302349	0.000479	0.001585
18	0.572175	0.573	0.000825	0.496	0.283799	0.284208	0.000409	0.00144
19	0.499539	0.499	0.000539	0.5119	0.255714	0.255438	0.000276	−0.00108
20	0.413485	0.413	0.000485	0.5265	0.2177	0.217445	0.000255	−0.00117
21	0.317161	0.3165	0.000661	0.5398	0.171204	0.170847	0.000357	−0.00209
22	0.212017	0.212	1.65E−05	0.5521	0.117054	0.117045	9.12E−06	−7.8E−05
23	0.102637	0.1035	0.000863	0.5633	0.057815	0.058302	0.000486	0.008343
24	−0.0093	−0.01	0.000701	0.5736	−0.00533	−0.00574	0.000402	0.070131
25	−0.12436	−0.123	0.001362	0.5833	−0.07254	−0.07175	0.000794	−0.01107
26	−0.2091	−0.21	0.000898	0.59	−0.12337	−0.1239	0.00053	0.004275
	IAE (Current)		1.7632E−02		**IAE (Power)**		6.480602E−03	
	SSE		1.55E−05		**RMSE**		7.72126E−04	
	MAE	6.78E−04	**MBE**	7.92E−08	**MAPE**	4.42293E−01		
	NMAE	4.72874E−05	NMBE	5.52585E−09	NRMSE	5.38404E−05		

Table 5
Optimal value of RTC. France Solar Cell (SDM) along with the comparison of Std., mean and min values of objective function with other MH algorithms.

S.No	Algorithm	N	RS	Rsh	Io	Iph	IAE	RMSE		
								Std	Mean	Min
1	HFGD	1.47727	0.03655	52.8899	0.31069	0.76079	0.017631849	**6.88E−18**	**7.73E−04**	**7.72E−04**
2	NRO-S (Wei et al., 2019)	1.4812	0.0364	53.7185	0.323	0.7608	–	2.87E−14	9.86E−04	9.86E−04
3	IWOA (Xiong et al., 2018a)	1.4812	0.0364	53.7317	0.3232	0.7608	0.0177034	1.13E−05	9.95E−04	9.86E−04
4	DE (Xiong et al., 2021)	1.4812	0.0364	53.7185	0.3231	0.7608	0.0181	6.72E−05	1.01E−03	9.86E−04
5	RTLBO (Xiong et al., 2018b)	1.4871	0.0361	55.3065	0.3423	0.7608	0.0217	3.06E−05	1.01E−03	9.86E−04
6	TLABC (Chen et al., 2018)	1.4812	0.0364	53.7164	0.3231	0.7608	0.0203	1.76E−05	9.98E−04	9.86E−04
7	BES (Nicaire et al., 2021)	1.4812	0.0364	53.7185	0.323	0.7607	0.0239	2.63E−13	9.86E−04	9.86E−04
8	HBA (Düzenli et al., 2022)	1.4812	0.0364	53.7185	0.323	0.7608	0.0256	7.81E−10	9.86E−04	9.86E−04
9	GOTLBO (Chen et al., 2016)	1.487	0.0362	53.8599	0.342	0.7608	0.0233	1.36E−04	1.09E−03	9.87E−04
10	HBO (AbdElminaam et al., 2022)	1.48003	0.0364	52.1563	0.319	0.76087	0.0219129	4.09E−04	1.51E−03	9.89E−04
11	NRO-P (Wei et al., 2019)	1.4799	0.0364	54.1619	0.3189	0.7608	–	6.63E−05	1.04E−03	9.88E−04

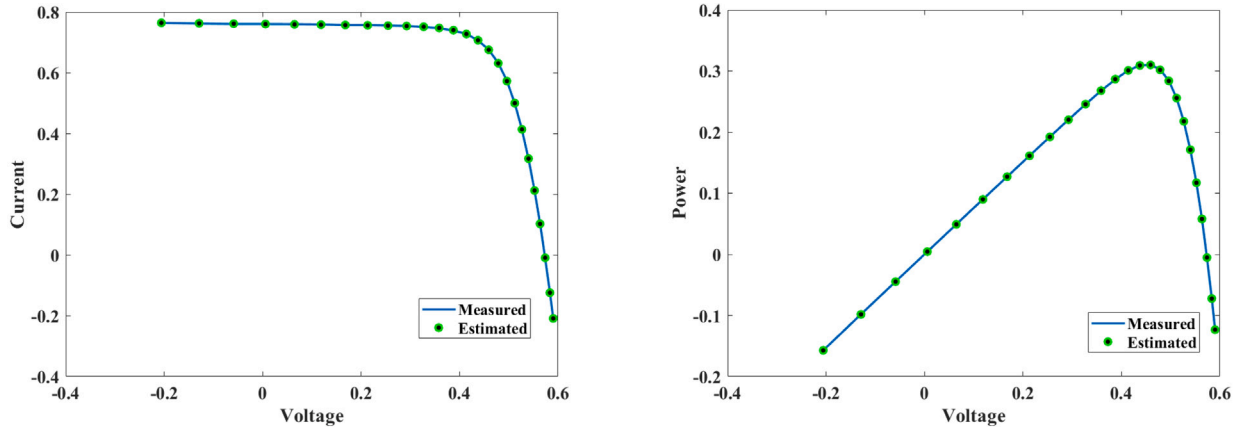

(a) IV characteristics for RTC (SDM) (b) PV characteristics for RTC (SDM)

Fig. 5. Estimated as well as measured solar cell IV and PV characteristics for RTC (SDM).

Table 6
The HFGD outcomes of Ie, IAE, MAE, MBE, MAPE, SSE, NMAE, NMBE, NRMSE, and RE for the RTC DDM.

S.No	Ie	Im	IAE	V	Pe	Pm	IAE	RE
1	0.764003035	0.764	3.03456E−06	−0.2057	−0.157155424	−0.1571548	6.24209E−07	−3.97194E−06
2	0.762620041	0.762	0.000620041	−0.1291	−0.098454247	−0.0983742	8.00473E−05	−0.000813702
3	0.761350426	0.7605	0.000850426	−0.0588	−0.044767405	−0.0447174	5.0005E−05	−0.001118245
4	0.760184292	0.7605	0.000315708	0.0057	0.00433305	0.00433485	1.79953E−06	0.000415132
5	0.759115385	0.76	0.000884615	0.0646	0.049038854	0.049096	5.71461E−05	0.001163967
6	0.758125283	0.759	0.000874717	0.1185	0.089837846	0.0899415	0.000103654	0.00115246
7	0.757186545	0.757	0.000186545	0.1678	0.127055902	0.1270246	3.13022E−05	−0.000246427
8	0.756234951	0.757	0.000765049	0.2132	0.161229292	0.1613924	0.000163108	0.001010633
9	0.755158688	0.7555	0.000341312	0.2545	0.192187886	0.19227475	8.68639E−05	0.00045177
10	0.753692858	0.754	0.000307142	0.2924	0.220379792	0.2204696	8.98083E−05	0.00040735
11	0.751357239	0.7505	0.000857239	0.3269	0.245618681	0.24533845	0.000280231	−0.001142224
12	0.747256521	0.7465	0.000756521	0.3585	0.267891463	0.26762025	0.000271213	−0.001013424
13	0.739966187	0.7385	0.001466187	0.3873	0.286588904	0.28602105	0.000567854	−0.001985358
14	0.727273694	0.728	0.000726306	0.4137	0.300873127	0.3011736	0.000300473	0.000997673
15	0.706892761	0.7065	0.000392761	0.4373	0.309124204	0.30895245	0.000171754	−0.000555925
16	0.675335114	0.6755	0.000164886	0.459	0.309978817	0.3100545	7.56828E−05	0.000244095
17	0.631018023	0.632	0.000981977	0.4784	0.301879022	0.3023488	0.000469778	0.001553761
18	0.572258412	0.573	0.000741588	0.496	0.283840173	0.284208	0.000367827	0.001294219
19	0.499639183	0.499	0.000639183	0.5119	0.255765298	0.2554381	0.000327198	−0.001280928
20	0.413553312	0.413	0.000553312	0.5265	0.217735819	0.2174445	0.000291319	−0.001339738
21	0.317170468	0.3165	0.000670468	0.5398	0.171208619	0.1708467	0.000361919	−0.002118384
22	0.21196713	0.212	3.28697E−05	0.5521	0.117027053	0.1170452	1.81473E−05	0.000155046
23	0.10255795	0.1035	0.00094205	0.5633	0.057770893	0.05830155	0.000530657	0.009101928
24	−0.009359782	−0.01	0.000640218	0.5736	−0.005368771	−0.005736	0.000367229	0.064021831
25	−0.124347306	−0.123	0.001347306	0.5833	−0.072531784	−0.0717459	0.000785884	−0.01095371
26	−0.208993675	−0.21	0.001006325	0.59	−0.123306269	−0.1239	0.000593731	0.004792022
	IAE (Current)			1.7067785E−02		**IAE (Power)**		6.445256 E-03
		SSE		1.45566E−05		**RMSE**		7.48245E−04
	MAE	6.82711E−04		**MBE**	−8.33602E−06		**MAPE**	04.20515087E−01
	NMAE	4.76056E−05		**NMBE**	−5.81272E−07		**NRMSE**	5.21752E−05

Table 7
Optimal value of RTC. France Solar Cell (DDM) along with the comparison of Std., mean and min values of objective function with other MH algorithms.

Sno	Algorithm	N1	N2	RS	Rsh	Io1	Io2	Iph	IAE	RMSE		
										Std	Mean	Min
1	HFGD	1.46395	2.34367	0.03682	54.784	0.26832	0.95332	0.76075	0.01706779	**4.72E−06**	**7.57E−04**	**7.48E−04**
2	ITLBO (Li et al., 2019b)	1.7892	1.4743	0.03614	53.7216	0.3204	0.8451	0.7608	1.91E−02	1.33E−05	9.80E−04	9.80E−04
3	TLABC (Chen et al., 2018)	1.9075	1.4567	0.0367	54.668	0.4239	0.2401	0.7608	1.97E−02	2.06E−05	9.80E−04	9.80E−04
4	DE (Xiong et al., 2021)	1.9974	1.4575	0.0366	54.3994	0.3564	0.5762	0.7608	2.28E−02	3.87E−05	9.90E−04	9.80E−04
5	RTLBO (Xiong et al., 2018b)	1.9614	1.4552	0.0363	49.085	0.2299	0.8527	0.7608	2.50E−02	1.95E−05	9.90E−04	9.80E−04
6	GOTLBO (Chen et al., 2016)	1.991	1.4638	0.0345	54.4147	0.341	0.2634	0.7608	2.87E−02	9.28E−05	1.00E−04	9.80E−04
7	GSK (Xiong et al., 2021)	1.9983	1.4627	0.0366	54.933	0.2595	0.4791	0.7608	2.97E−02	8.72E−07	9.80E−04	9.80E−04
8	IWOA (Xiong et al., 2018a)	1.4545	2	0.0367	55.4082	0.6771	0.2355	0.7608	1.73E−02	1.92E−05	9.97E−04	9.83E−04
9	HBA (Düzenli et al., 2022)	2	1.453	0.0367	55.264	0.2316	0	0.7608	2.30E−02	1.50E−07	9.82E−04	9.83E−04
10	HBA-OBL (Düzenli et al., 2022)	1.4545	2	0.0367	55.3172	0.6713	0	0.7608	2.54E−02	1.87E−07	9.83E−04	9.83E−04
11	NRO-S (Wei et al., 2019)	1.9615	1.4797	0.0364	53.8266	0.0433	0.0317	0.7608	–	9.06E−06	1.02E−03	9.86E−04
12	NRO-P (Wei et al., 2019)	1.4809	1.0017	0.0364	50.5576	0.3221	0	0.7613	–	1.55E−03	3.30E−04	1.02E−03
13	HBO (AbdElminaam et al., 2022)	1.44075	1.90873	0.0368	51.6762	0.674	0.197	0.7607	2.33E−02	3.86E−04	1.56E−03	1.05E−03
14	WOA (Xiong et al., 2018a)	1.7961	1.497	0.0354	55.5644	0.365	0.1274	0.7611	1.94E−02	1.66E−03	3.35E−03	1.13E−03

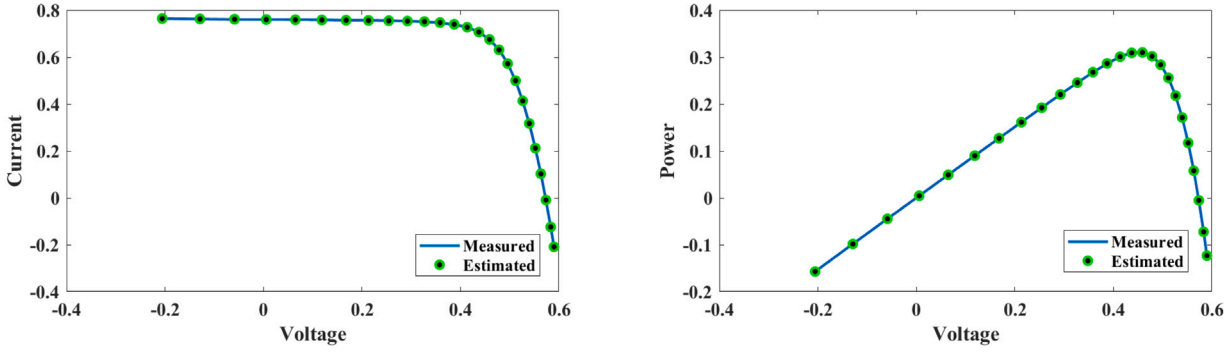

(a) IV characteristics for RTC (DDM) (b) PV characteristics for RTC (DDM)

Fig. 6. Estimated as well as measured solar cell IV and PV characteristics for RTC (DDM).

Table 8
The HFGD outcomes of Ie, IAE, MAE, MBE, MAPE, SSE, NMAE, NMBE, NRMSE, and RE for the Amorphous Silicon aSi:H.

Sno	Ie	Im	IAE	V	Pe	Pm	IAE	RE
1	0.011364	0.011283	8.08E−05	−0.01	−0.00011	−0.00011	8.08E−07	−0.00716
2	0.011328	0.011266	6.28E−05	0.00848	9.61E−05	9.55E−05	5.33E−07	−0.00558
3	0.011293	0.011243	5.04E−05	0.026955	0.000304	0.000303	1.36E−06	−0.00449
4	0.011257	0.011224	3.38E−05	0.045435	0.000511	0.00051	1.53E−06	−0.00301
5	0.011222	0.011202	1.93E−05	0.063915	0.000717	0.000716	1.24E−06	−0.00173
6	0.011186	0.011193	7.03E−06	0.08239	0.000922	0.000922	5.8E−07	0.000628
7	0.01115	0.011155	4.41E−06	0.10087	0.001125	0.001125	4.45E−07	0.000396
8	0.011114	0.01111	4E-06	0.11935	0.001327	0.001326	4.78E−07	−0.00036
9	0.011078	0.011099	2.06E−05	0.137825	0.001527	0.00153	2.84E−06	0.001857
10	0.011042	0.011078	3.6E−05	0.156305	0.001726	0.001732	5.63E−06	0.003249
11	0.011006	0.01104	3.39E−05	0.174785	0.001924	0.00193	5.92E−06	0.003069
12	0.010969	0.011007	3.78E−05	0.19326	0.00212	0.002127	7.31E−06	0.003435
13	0.010932	0.010982	4.94E−05	0.21175	0.002315	0.002325	1.05E−05	0.004497
14	0.010895	0.010941	4.64E−05	0.2302	0.002508	0.002519	1.07E−05	0.004238
15	0.010857	0.010896	3.91E−05	0.2487	0.0027	0.00271	9.73E−06	0.003592
16	0.010819	0.010861	4.23E−05	0.26715	0.00289	0.002902	1.13E−05	0.003894
17	0.01078	0.010838	5.8E−05	0.28565	0.003079	0.003096	1.66E−05	0.005352
18	0.010739	0.010777	3.79E−05	0.30415	0.003266	0.003278	1.15E−05	0.003518
19	0.010698	0.010724	2.52E−05	0.3226	0.003451	0.003459	8.14E−06	0.002354
20	0.010656	0.01069	3.4E−05	0.3411	0.003635	0.003646	1.16E−05	0.00318
21	0.010611	0.010624	1.24E−05	0.35955	0.003815	0.00382	4.44E−06	0.001163
22	0.010565	0.010596	3.11E−05	0.37805	0.003994	0.004006	1.17E−05	0.002933
23	0.010516	0.010523	6.82E−06	0.3965	0.00417	0.004172	2.71E−06	0.000648
24	0.010463	0.010467	3.79E−06	0.415	0.004342	0.004344	1.57E−06	0.000362
25	0.010407	0.010407	5.37E−07	0.4335	0.004511	0.004512	2.33E−07	5.16E−05
26	0.010345	0.010327	1.81E−05	0.45195	0.004676	0.004667	8.2E−06	−0.00176
27	0.010278	0.010258	2E-05	0.47045	0.004835	0.004826	9.42E−06	−0.00195
28	0.010202	0.010173	2.97E−05	0.4889	0.004988	0.004973	1.45E−05	−0.00292
29	0.010117	0.01006	5.72E−05	0.5074	0.005133	0.005104	2.9E−05	−0.00569
30	0.01002	0.009967	5.34E−05	0.52585	0.005269	0.005241	2.81E−05	−0.00535
31	0.009909	0.009853	5.53E−05	0.54435	0.005394	0.005364	3.01E−05	−0.00562
32	0.009779	0.009702	7.68E−05	0.56285	0.005504	0.005461	4.33E−05	−0.00792
33	0.009627	0.009567	6.02E−05	0.5813	0.005596	0.005561	3.5E−05	−0.00629
34	0.009447	0.009384	6.32E−05	0.5998	0.005666	0.005628	3.79E−05	−0.00674
35	0.009233	0.009201	3.2E−05	0.61825	0.005708	0.005689	1.98E−05	−0.00347
36	0.008976	0.008975	1.11E−06	0.63675	0.005715	0.005715	7.09E−07	−0.00012
37	0.008667	0.008685	1.85E−05	0.6552	0.005678	0.005691	1.21E−05	0.002128
38	0.008292	0.008338	4.61E−05	0.6737	0.005586	0.005617	3.1E−05	0.005525
39	0.007837	0.007911	7.44E−05	0.69215	0.005424	0.005476	5.15E−05	0.009405
40	0.00728	0.007373	9.22E−05	0.71065	0.005174	0.005239	6.55E−05	0.012508
41	0.0066	0.006665	6.52E−05	0.72915	0.004812	0.00486	4.75E−05	0.009781
42	0.005768	0.005787	1.89E−05	0.7476	0.004312	0.004326	1.41E−05	0.00327
43	0.004744	0.004701	4.26E−05	0.7661	0.003634	0.003602	3.27E−05	−0.00907
44	0.003488	0.003403	8.47E−05	0.78455	0.002737	0.00267	6.65E−05	−0.02489
45	0.001938	0.001877	6.06E−05	0.80305	0.001556	0.001507	4.87E−05	−0.03229
46	3.15E−05	9.58E−05	6.43E−05	0.8215	2.59E−05	7.87E−05	5.28E−05	0.671148
	IAE (Current)		1.812E−03		**IAE (Power)**		8.17813E−04	
	SSE		9.79E−08		**RMSE**		4.61E−05	
	MAE	3.94E−05		**MBE**	7.55E−13		**MAPE**	1.953447
	NMAE	9.05E−05		**NMBE**	1.73E−12		**NMRSE**	1.06 E-04

Table 9
Optimal value of Amorphous Silicon aSi:H along with the comparison of Std., mean and min values of objective function with other MH algorithms.

S.No	Algorithm	N	RS	Rsh	Io	Iph	IAE	Std	Mean	Min
								RMSE		
1	HFGD	3.36842	2.17E−13	523.154	0.73494	0.01134	0.00181	6.30E−20	4.61E−05	4.61E−05
2	HSDA (Cotfas et al., 2021)	3.35383	0.04028	520.065	0.70475	0.01134	0.00182	NA	NA	4.62E−05
3	BMOA (Madhiarasan et al., 2022)	3.7077	0	7.293	1.7698	0.011235	0.003198	NA	NA	8.21E−05
4	SDA (Cotfas et al., 2019)	1.679294	0.091316	99.13667	0.516854	0.425752	NA	NA	NA	5.63E−04
5	GA (Cotfas et al., 2019)	1.73926	0.085944	123.3659	0.838331	0.425688	NA	NA	NA	6.97E−04
6	5P (Madhiarasan et al., 2022) (Cotfas et al., 2019)	1.618311	0.103522	145.222	0.306456	0.4255	0.008738	NA	NA	2.26E−03

5.2.4. Parameter extraction of PVM 752 GaAs thin-film

The PVM 752 GaAs thin film solar cell is tested at a temperature of 25 °C and an irradiance of 1000 W/m^2 in order to determine the unknown parameters using the HFGD algorithm. The data sheet containing the measured data of the PVM 752 GaAs solar PV cell, including a total of 44 I–V tested samples, has been obtained from Ali et al. (2023), Lekouaghet et al. (2021). The best $IAE_{current}$, as well as IAE_{power}, SSE, RMSE, MAPE, MBE, NMAE, NMBE, NRMSE, and Im, are

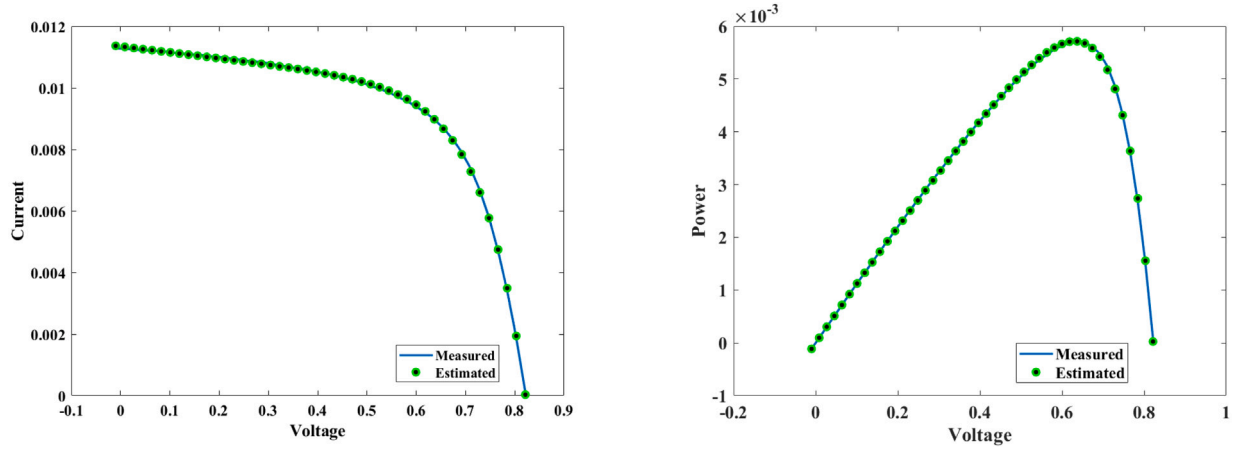

(a) IV characteristics for Amorphous Silicon aSi:H (b) PV characteristics for Amorphous Silicon aSi:H

Fig. 7. Estimated as well as measured solar module IV and PV characteristics for Amorphous Silicon aSi:H.

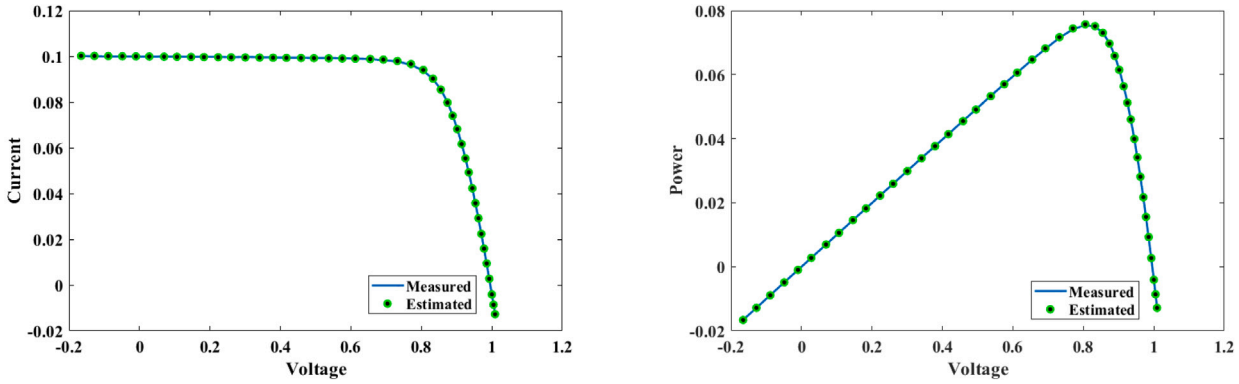

(a) IV characteristics for PVM 752 GaAs Thin-Film (b) PV characteristics for PVM 752 GaAs Thin-Film

Fig. 8. Estimated as well as measured solar module IV and PV characteristics for PVM 752 GaAs Thin-Film.

displayed in Table 10. The best $IAE_{current}$, and IAE_{power} are 0.006053 and 0.004021, respectively. The best RMSE values for PVM 752 GaAs Thin-Film (1.59E−04) are demonstrated in Table 11. For this model, the HFGD algorithm obtains the best value of the RMSE. In addition, the HFGD algorithm optimum value of unknown parameters of this model along with the comparison of obtained outcomes with other MH algorithms in Table 11. Furthermore, the accuracy of the HFGD algorithm is displayed in the well-known IV and PV curve of the PV module is given in Figs. 8(a) and 8(b).

5.2.5. Statistical validations

This section presents statistical analysis (Friedman and Wilcoxon tests) based on min value of RMSE for the HFGD algorithm for 30 runs. From statistical analysis, it is observed that the proposed algorithm gives robustness and accuracy over other MH algorithms. The boxplot of the solar PV cells/modules (SDM, DDM, Amorphous Silicon aSi:H and PVM 752 GaAs thin-film) as shown in Figs. 9(a), 9(b), 9(c) and 9(d), respectively. Tables 12–15 illustrates the average ranks, R^+, p values, as well as R^- for the proposed and compared algorithms using solar PV cell/module (SDM, DDM, Amorphous Silicon aSi:H and PVM 752 GaAs thin-film) challenges, based on the Friedman and Wilcoxon tests. Depending on these test results, the HFGD has got the highest rank (1st rank) in all the cases, displayed in Tables 12, 13, 14 and 15, respectively. In comparison with other MH algorithms, the HFGD algorithm achieves greater R^+ values than R^- in each of the solar PV cells/modules challenges are tabulated in the Tables 12, 13, 14 and 15, respectively. The results demonstrated that the HFGD algorithm outperforms previous MH approaches in solving all solar PV cells/modules challenges.

6. Discussion

This section is divided into three subsections, where the first part deals with the overall summary of the paper, the second part gives emphasis on the drawbacks of the proposed approach and finally in the third subsection some future insightful implications are presented. The details are as

6.1. Summary of results

A multi-hybrid algorithm using the best known properties of FPA, GWO and DE, namely HFGD is proposed. The algorithm employs iterative division, adaptive switching, and population adaptation, for improved performance. The algorithm is self-adaptive in nature, and hence no user based parametric tuning is required. The proposed HFGD is tested on CEC 2019 benchmark dataset, and it has been found that the algorithm perform significantly better with respect to previous competition winners including jDE100, YDSE, among others. Along with the benchmark challenges, parameter estimation of solar PV (SDM, DDM, Amorphous Silicon aSi:H and PVM 752 GaAs thin-film cell/module) utilizing the HFGD algorithm shows that the proposed algorithm achieves noticeably superior outcomes in comparison with the existing MH algorithms. Also, the HFGD algorithm is demonstrably

Table 10
The HFGD outcomes of Ie, IAE, MAE, MBE, MAPE, SSE, NMAE, NMBE, NRMSE, and RE for the PVM 752 GaAs Thin-Film.

S.No	Ie	Im	IAE	V	Pe	Pm	IAE	RE
1	0.100192	0.1001	9.24E−05	−0.1659	−0.01662	−0.01661	1.53E−05	−0.00092
2	0.100135	0.1	0.000135	−0.1281	−0.01283	−0.01281	1.73E−05	−0.00135
3	0.100076	0.0999	0.000176	−0.0888	−0.00889	−0.00887	1.56E−05	−0.00176
4	0.100016	0.0999	0.000116	−0.049	−0.0049	−0.0049	5.68E−06	−0.00116
5	0.099957	0.0999	5.72E−05	−0.0102	−0.00102	−0.00102	5.83E−07	−0.00057
6	0.0999	0.0998	0.0001	0.0275	0.002747	0.002745	2.76E−06	−0.001
7	0.099837	0.0999	6.32E−05	0.0695	0.006939	0.006943	4.39E−06	0.000633
8	0.099782	0.0998	1.85E−05	0.1061	0.010587	0.010589	1.96E−06	0.000185
9	0.099721	0.0998	7.88E−05	0.146	0.014559	0.014571	1.15E−05	0.000789
10	0.099666	0.0997	3.44E−05	0.1828	0.018219	0.018225	6.28E−06	0.000345
11	0.099605	0.0997	9.51E−05	0.223	0.022212	0.022233	2.12E−05	0.000954
12	0.099549	0.0996	5.1E−05	0.26	0.025883	0.025896	1.33E−05	0.000512
13	0.099488	0.0997	0.000212	0.3001	0.029856	0.02992	6.35E−05	0.002123
14	0.099427	0.0996	0.000173	0.3406	0.033865	0.033924	5.89E−05	0.001736
15	0.099369	0.0995	0.000131	0.3789	0.037651	0.037701	4.96E−05	0.001315
16	0.099312	0.0994	8.85E−05	0.4168	0.041393	0.04143	3.69E−05	0.00089
17	0.099248	0.0994	0.000152	0.4583	0.045485	0.045555	6.97E−05	0.00153
18	0.099191	0.0993	0.000109	0.4949	0.049089	0.049144	5.42E−05	0.001102
19	0.099121	0.0993	0.000179	0.537	0.053228	0.053324	9.61E−05	0.001803
20	0.099049	0.0992	0.000151	0.5753	0.056983	0.05707	8.66E−05	0.001518
21	0.098961	0.099	3.85E−05	0.6123	0.060594	0.060618	2.36E−05	0.000389
22	0.098804	0.0988	4.46E−06	0.6546	0.064677	0.064674	2.92E−06	−4.5E−05
23	0.098544	0.0983	0.000244	0.6918	0.068172	0.068004	0.000168	−0.00248
24	0.097944	0.0977	0.000244	0.7318	0.071675	0.071497	0.000178	−0.00249
25	0.096628	0.0963	0.000328	0.7702	0.074423	0.07417	0.000253	−0.00341
26	0.094022	0.0937	0.000322	0.8053	0.075716	0.075457	0.00026	−0.00344
27	0.090209	0.09	0.000209	0.8329	0.075135	0.074961	0.000174	−0.00233
28	0.08542	0.0855	7.96E−05	0.855	0.073034	0.073103	6.81E−05	0.000932
29	0.079754	0.0799	0.000146	0.8738	0.069689	0.069817	0.000128	0.001831
30	0.074051	0.0743	0.000249	0.8887	0.065809	0.06603	0.000221	0.003347
31	0.06818	0.0683	0.00012	0.9016	0.061471	0.061579	0.000108	0.001757
32	0.061639	0.0618	0.000161	0.9141	0.056344	0.056491	0.000147	0.00261
33	0.055373	0.0555	0.000127	0.9248	0.051209	0.051326	0.000118	0.002291
34	0.049238	0.0493	6.25E−05	0.9344	0.046008	0.046066	5.84E−05	0.001268
35	0.042275	0.0422	7.45E−05	0.9445	0.039928	0.039858	7.04E−05	−0.00177
36	0.0358	0.0357	9.97E−05	0.9533	0.034128	0.034033	9.5E−05	−0.00279
37	0.029201	0.0291	0.000101	0.9618	0.028086	0.027988	9.72E−05	−0.00347
38	0.022364	0.0222	0.000164	0.9702	0.021697	0.021538	0.000159	−0.00737
39	0.01592	0.0157	0.00022	0.9778	0.015566	0.015351	0.000215	−0.014
40	0.009422	0.0092	0.000222	0.9852	0.009283	0.009064	0.000219	−0.02416
41	0.002716	0.0026	0.000116	0.9926	0.002696	0.002581	0.000115	−0.04454
42	−0.00409	−0.004	9.39E−05	0.9999	−0.00409	−0.004	9.39E−05	−0.02348
43	−0.00858	−0.0085	7.54E−05	1.0046	−0.00861	−0.00854	7.57E−05	−0.00887
44	−0.01274	−0.0124	0.000339	1.0089	−0.01285	−0.01251	0.000342	−0.02733
	IAE (Current)		6.053E−03		**IAE (Power)**		4.021354E−03	
	SSE		1.12E−06		**RMSE**		1.59243E−04	
	MAE	**1.38E−04**		**MBE**	7.89E−08		**MAPE**	4.74094E−01
	NMAE	**4.20224E−05**		**NMBE**	2.41097E−08		**NRMSE**	4.86431E−05

Table 11
Optimal value of PVM 752 GaAs Thin-Film along with the comparison of Std., mean and min values of objective function with other MH algorithms.

S. No	Algorithm	N	RS	Rsh	Io1	Iph	IAE	Std	Mean	Min
								RMSE		
1	HFGD	1.662595269	0.641599	661.2761442	7.45E−06	0.100039	0.006053	2.29E−07	1.59E−04	1.59E−04
2	ELBA (Deotti et al., 2020)	1.61568	0.66051	608.01	3.78E−04	0.10007	NA	3.57E−18	2.28E−04	2.28E−04
3	DBA (Deotti et al., 2020)	1.624056	661.3119	661.311949	4.28E−06	0.100022	NA	1.50E−04	4.38E−04	2.29E−04
4	IJAYA (Jordehi, 2018)	1.88746	0.5	100	1.13E−10	0.103253	NA	1.16E−05	2.54E−04	2.29E−04
5	SDO (Xiong et al., 2019)	1.6467	0.6499	668.5946	5.94E−06	0.1	0.005935	2.77E−05	3.17E−04	2.37E−04
6	NBA (Deotti et al., 2020)	1.801044	0.595697	1000	4.49E−05	0.099975	NA	8.60E−05	5.95E−04	3.95E−04
7	LCROA (Lekouaghet et al., 2021)	1.87845	0.57044	842.475	1.09E−04	0.09997	NA	7.28E−02	4.87E−02	7.61E−04
8	CNMSMA (Liu et al., 2021)	1.840868	0.5	100	6.76E−05	0.103312	NA	1.95E−13	2.26E−03	2.26E−03
9	BA (Deotti et al., 2020)	1.79958	0.217866	789.910856	3.84E−05	0.091125	NA	5.58E−02	8.01E−02	8.60E−03
10	ELPSO (Jordehi, 2018)	1.76859	0.159052	14.429507	0	0.115016	NA	0	2.54E−02	2.54E−02

superior to other recently proposed parameter extraction strategies in terms of accuracy, stability, and speed, according to the outcomes of the experiments. Additionally, the competition outcomes and statistics rates show that the HFGD algorithm developed in this analysis is capable of accurately and successfully identifying solar PV parameters. Statistically, Wilcoxon and Freidmann tests further prove the

Table 12
Friedman's rank and Wilcoxon test for R.T.C France Solar Cell (SDM).

S.No	R.T.C France Solar Cell (SDM)						
	Algorithm	Friedman's rank	Rank	R+	R−	*p value*	Result
1	HFGD	1.34771267	**1**				
2	NRO-S	4.32959967	4	465	0	1.69E−14	+
3	IWOA	6.46048669	5	465	0	1.18E−12	+
4	DE	7.55873774	7	465	0	1.01E−12	+
5	RTLBO	8.23034422	8	465	0	1.17E−12	+
6	TLABC	7.39447314	6	465	0	1.13E−12	+
7	BES	3.15152	2	465	0	7.91E−13	+
8	HBA	3.82678969	3	465	0	3.37E−13	+
9	GOTLBO	9.47143114	10	465	0	1.10E−12	+
10	HBO	11.3412579	11	465	0	1.21E−12	+
11	NRO-P	8.7533858	9	465	0	1.18E−12	+

Table 13
Friedman's rank and Wilcoxon test for R.T.C France Solar Cell (DDM).

S.No	R.T.C France Solar Cell (DDM)						
	Algorithm	Friedman's rank	Rank	R+	R−	*p value*	Result
1	HFGD	1.80979913	**1**				
2	ITLBO	7.45204232	9	465	0	2.91E−11	+
3	TLABC	5.36694714	3	465	0	2.50E−11	+
4	DE	6.94188634	5	465	0	2.99E−11	+
5	RTLBO	7.02176128	8	465	0	3.01E−11	+
6	GOTLBO	7.01573553	7	465	0	2.39E−11	+
7	GSK	5.058874	2	465	0	2.99E−11	+
8	IWOA	9.22615909	10	465	0	3.02E−11	+
9	HBA	6.9557407	6	465	0	2.96E−11	+
10	HBA-OBL	6.13571168	4	465	0	2.97E−11	+
11	NRO-S	11.0824626	11	465	0	3.02E−11	+
12	NRO-P	12.4673266	12	465	0	8.34E−09	+
13	HBO	13.3120685	13	465	0	3.02E−11	+
14	WOA	14.3244068	14	465	0	3.02E−11	+

Table 14
Friedman's rank and Wilcoxon test for Amorphous Silicon aSi:H.

S.No	Amorphous Silicon aSi:H						
	Algorithm	Friedman's rank	Rank	R+	R−	*p value*	Result
1	HFGD	1.15761308	**1**				
2	HSDA	2.0975404	2	465	0	2.01E−13	+
3	BMOA	3.27849822	3	465	0	1.97E−13	+
4	SDA	4.88021485	4	465	0	1.55E−13	+
5	GA	5.75750684	5	465	0	5.59E−13	+
6	5P	6.8315552	6	465	0	3.37E−13	+

Table 15
Friedman's rank and Wilcoxon test for PVM 752 GaAs Thin-Film.

S.No	PVM 752 GaAs Thin-Film						
	Algorithm	Friedman's rank	Rank	R+	R−	*p value*	Result
1	HFGD	1.97974838	**1**				
2	SDO	4.94805702	4	465	0	2.94E−11	+
3	ELBA	2.90579194	2	465	0	1.64E−11	+
4	DBA	4.82698682	5	465	0	2.93E−11	+
5	IJAYA	4.18004252	3	465	0	2.94E−11	+
6	NBA	6.56569258	6	465	0	2.94E−11	+
7	LCROA	8.86420707	8	465	0	2.84E−11	+
8	CNMSMA	7.57849822	7	465	0	1.86E−11	+
9	BA	9.91354819	10	465	0	2.94E−11	+
10	ELPSO	9.49084017	9	465	0	1.17E−12	+

significance of the proposed HFGD algorithm. Overall, the enhanced performance of HFGD is due to the added advantages of FPA, GWO, and DE. The addition of adaptive properties makes the algorithm self-sufficient, and hence helps in avoiding local optima stagnation and other problems.

6.2. Drawbacks

The proposed HFGD is found to be highly competitive, but as the problem complexity increases, it is found to provide stagnating results. This might be due to the poor *expt* operation and hence more significant

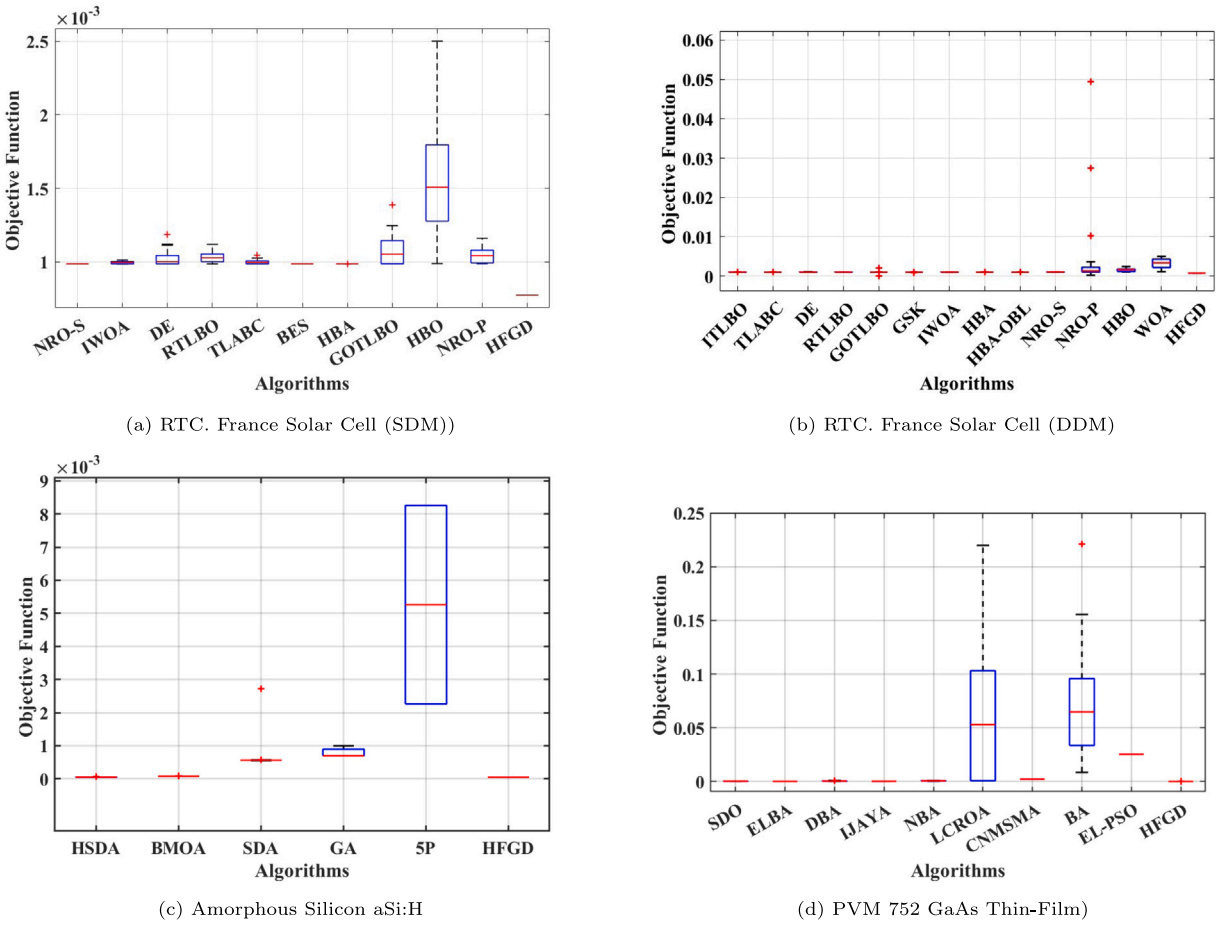

(a) RTC. France Solar Cell (SDM))

(b) RTC. France Solar Cell (DDM)

(c) Amorphous Silicon aSi:H

(d) PVM 752 GaAs Thin-Film)

Fig. 9. Boxplot for RTC. France Solar Cell (SDM), RTC. France Solar Cell (DDM), Amorphous Silicon aSi:H, and PVM 752 GaAs Thin-Film.

search needs to be added. Though population adaptation has been added to reduce the computational burden, but it is very tricky to use such a strategy. The population size can reduce abruptly if the solution is changing very fast and this can lead to poor stability and hence chances of getting stuck in some local optima is more.A balance in *expl* and *expt* is still a matter of concern for this algorithm. This can be found from the convergence profiles that the algorithm does not give optimal convergence patterns and hence rigorous studies are required. A very important point that still needs to be addressed is that the algorithm does not provide good results for all the problems under consideration. This may due to local optima stagnation in some of the cases, and hence more work is required to enhance the overall performance of the algorithm.

6.3. Insightful implications

The *expt* operation thus must be enhanced by using a set of new equations and also multiple different mutation/inertia weight operators. Better and enhanced operation for population adaptation can be added to make the algorithm more stable and have a reduced computational burden. A deeper analysis of the proposed algorithm must be done with respect to variable population strategies must be done for enhanced performance. Even though new search strategies have been added, it is still a concern how the algorithm behaves for binary and discrete set of problems. The algorithm can be exploited for these problems and see how it behaves. The algorithm is self-adaptive in nature and hence can be extended to various domain research problems including medical imaging, antenna arrays, segmentation among others. Apart from that, theoretical foundations of the proposed algorithm can be studied and empirical studies on the stability and convergence patterns can be drawn for better understanding of the proposed HFGD algorithm.

7. Conclusions

This paper proposed a hybrid algorithm called HFGD based on the hybrid properties of DE, FPA, and GWO. The algorithm uses a combination of equations, self-adaptive parameters, iterative division, population division, and population adaptation to look for the best possible solutions. The comparative results on the CEC 2019 benchmark dataset and statistical tests show that HFGD is a highly competitive algorithm and can be considered a potential candidate for high-dimensional problems. The proposed HFGD algorithm is applied to estimate the five unknown parameters (R_s, N, I_{sc}, R_{shu}, and I_{Ph}) for SDM and seven unknown parameters (R_s, N_1 and N_2, I_{sc1}, I_{sc2}, R_{shu}, and I_{Ph}) for DDM of PV cells/modules. Many cases have been used to illustrate the algorithm's performance, including SDM, DDM, Amorphous Silicon aSi:H, and PVM 752 GaAs thin-film. When compared to other MH optimization techniques, HFGD algorithm achieves dramatically lower IAE and objective function values with superior robustness. For the SDM, DDM, Amorphous Silicon aSi:H, and PVM 752 GaAs Thin-Film, the HFGD algorithm can minimize the objective function to 7.72E−04, 7.48E−04, 4.61E−05 as well as 1.59E−04, respectively. Furthermore, the I–V and P–V characteristics of the measured and estimated data demonstrate the presented method's accuracy.

In addition, the accuracy and robustness of the HFGD algorithm are evaluated statistically by utilizing Friedman's rank and Wilcoxon test. In all the cases, the proposed algorithm rank is on top as compared with the other MH algorithms. Finally, the research outcomes indicate that the proposed HFGD algorithm displays a high level of reliability

and simplicity as an optimization tool for addressing PV parameter estimation problems. Future research will involve the application of HFGD algorithm to the solving of constrained and multi-objective optimization challenges in a variety of disciplines. Also, future works will focus on enhancing the use of the MH algorithm for solving complex power systems (energy scheduling, as well as energy management etc.) and maximum power point tracking challenges.

CRediT authorship contribution statement

Pankaj Sharma: Writing – original draft, Data curation, Software, Validation, Result and discussion, Real-world application. **Saravanakumar Raju:** Supervision, Reviewing and editing, Project administration, Resources. **Rohit Salgotra:** Conceptualization, Methodology, Data curation, Writing – original draft, Supervision, Project administration, Resources, Reviewing and editing. **Amir H. Gandomi:** Supervision, Reviewing and editing, Project administration, Resources.

Declaration of competing interest

The authors declare that they have no known competing financial interests or personal relationships that could have appeared to influence the work reported in this paper.

Data availability

No data was used for the research described in the article.

Acknowledgment

Amir H Gandomi would like to thank University Research and Innovation Center (EKIK), Obuda University, Budapest, Hungary, for providing the required funding and support to publish this paper.

References

Abbas, M.K., Hassan, Q., Tabar, V.S., Tohidi, S., Jaszczur, M., Abdulrahman, I.S., Salman, H.M., 2023. Techno-economic analysis for clean hydrogen production using solar energy under varied climate conditions. Int. J. Hydrogen Energy 48 (8), 2929–2948.

Abbassi, R., Abbassi, A., Jemli, M., Chebbi, S., 2018. Identification of unknown parameters of solar cell models: A comprehensive overview of available approaches. Renew. Sustain. Energy Rev. 90, 453–474.

Abd El-Mageed, A.A., Abohany, A.A., Saad, H.M., Sallam, K.M., 2023. Parameter extraction of solar photovoltaic models using queuing search optimization and differential evolution. Appl. Soft Comput. 134, 110032.

Abd Elaziz, M., Sarkar, U., Nag, S., Hinojosa, S., Oliva, D., 2020. Improving image thresholding by the type II fuzzy entropy and a hybrid optimization algorithm. Soft Comput. 1–21.

Abdel-Basset, M., El-Shahat, D., Chakrabortty, R.K., Ryan, M., 2021. Parameter estimation of photovoltaic models using an improved marine predators algorithm. Energy Convers. Manage. 227, 113491.

Abdel-Basset, M., El-Shahat, D., Jameel, M., Abouhawwash, M., 2023. Young's double-slit experiment optimizer: A novel metaheuristic optimization algorithm for global and constraint optimization problems. Comput. Methods Appl. Mech. Engrg. 403, 115652.

AbdElminaam, D.S., Houssein, E.H., Said, M., Oliva, D., Nabil, A., 2022. An efficient heap-based optimizer for parameters identification of modified photovoltaic models. Ain Shams Eng. J. 13 (5), 101728.

Ahmad, M.F., Isa, N.A.M., Lim, W.H., Ang, K.M., 2022. Differential evolution: A recent review based on state-of-the-art works. Alex. Eng. J. 61 (5), 3831–3872.

Ali, F., Sarwar, A., Bakhsh, F.I., Ahmad, S., Shah, A.A., Ahmed, H., 2023. Parameter extraction of photovoltaic models using atomic orbital search algorithm on a decent basis for novel accurate RMSE calculation. Energy Convers. Manage. 277, 116613.

Anjaneya Vara Prasad, P., Dhanamjayulu, C., et al., 2023. An overview on multi-level inverter topologies for grid-tied PV system. Int. Trans. Electr. Energy Syst. 2023.

Askarzadeh, A., Rezazadeh, A., 2012. Parameter identification for solar cell models using harmony search-based algorithms. Sol. Energy 86 (11), 3241–3249.

Ayyarao, T.S., Kishore, G.I., 2023. Parameter estimation of solar PV models with artificial humming bird optimization algorithm using various objective functions. Soft Comput. 1–22.

Bati, A.S., Zhong, Y.L., Burn, P.L., Nazeeruddin, M.K., Shaw, P.E., Batmunkh, M., 2023. Next-generation applications for integrated perovskite solar cells. Commun. Mater. 4 (1), 2.

Beşkirli, A., Dağ, İ., 2022. An efficient tree seed inspired algorithm for parameter estimation of photovoltaic models. Energy Rep. 8, 291–298.

Brest, J., Maučec, M.S., Bošković, B., 2019. The 100-digit challenge: Algorithm jde100. In: 2019 IEEE Congress on Evolutionary Computation. (CEC), IEEE, pp. 19–26.

Chauhan, A., Prakash, S., 2023. Optimal parameter estimation of solar photovoltaics through nature inspired metaheuristic and hybrid approaches. IETE J. Res. 1–19.

Chen, C., Ge, Z., Zhang, Y., 2023. Study of combined heat and power plant integration with thermal energy storage for operational flexibility. Appl. Therm. Eng. 219, 119537.

Chen, X., Xu, B., Mei, C., Ding, Y., Li, K., 2018. Teaching-learning-based artificial bee colony for solar photovoltaic parameter estimation. Appl. Energy 212, 1578–1588.

Chen, X., Yu, K., Du, W., Zhao, W., Liu, G., 2016. Parameters identification of solar cell models using generalized oppositional teaching learning based optimization. Energy 99, 170–180.

Chowdhury, T.A., Zafar, M.A.B., Islam, M.S.-U., Shahinuzzaman, M., Islam, M.A., Khandaker, M.U., 2023. Stability of perovskite solar cells: issues and prospects. RSC Adv. 13 (3), 1787–1810.

Cotfas, D.T., Deaconu, A.M., Cotfas, P.A., 2019. Application of successive discretization algorithm for determining photovoltaic cells parameters. Energy Convers. Manage. 196, 545–556.

Cotfas, D.T., Deaconu, A.M., Cotfas, P.A., 2021. Hybrid successive discretisation algorithm used to calculate parameters of the photovoltaic cells and panels for existing datasets. IET Renew. Power Gener. 15 (15), 3661–3687.

Deotti, L.M.P., Pereira, J.L.R., da Silva Junior, I.C., 2020. Parameter extraction of photovoltaic models using an enhanced Lévy flight bat algorithm. Energy Convers. Manage. 221, 113114.

Düzenli, T., Onay, F., Aydemir, S., 2022. Improved honey badger algorithms for parameter extraction in photovoltaic models. Optik 268, 169731.

Hassan, S., Hemeida, A.M., Alkhalaf, S., Mohamed, A.-A., Senjyu, T., 2020. Multi-variant differential evolution algorithm for feature selection. Sci. Rep. 10 (1), 1–16.

Jordehi, A.R., 2016. Parameter estimation of solar photovoltaic (PV) cells: A review. Renew. Sustain. Energy Rev. (ISSN: 1364-0321) 61, 354–371.

Jordehi, A.R., 2018. Enhanced leader particle swarm optimisation (ELPSO): An efficient algorithm for parameter estimation of photovoltaic (PV) cells and modules. Sol. Energy 159, 78–87.

Lekouaghet, B., Boukabou, A., Boubakir, C., 2021. Estimation of the photovoltaic cells/modules parameters using an improved rao-based chaotic optimization technique. Energy Convers. Manage. 229, 113722.

Li, S., Gong, W., Yan, X., Hu, C., Bai, D., Wang, L., 2019a. Parameter estimation of photovoltaic models with memetic adaptive differential evolution. Sol. Energy 190, 465–474.

Li, S., Gong, W., Yan, X., Hu, C., Bai, D., Wang, L., Gao, L., 2019b. Parameter extraction of photovoltaic models using an improved teaching-learning-based optimization. Energy Convers. Manage. 186, 293–305.

Liu, Y., Heidari, A.A., Ye, X., Liang, G., Chen, H., He, C., 2021. Boosting slime mould algorithm for parameter identification of photovoltaic models. Energy 234, 121164.

Liu, Y., Tan, X., Liang, J., Han, H., Xiang, P., Yan, W., 2023. Machine learning for perovskite solar cells and component materials: key technologies and prospects. Adv. Funct. Mater. 2214271.

Maden, D., Çelik, E., Houssein, E.H., Sharma, G., 2023. Squirrel search algorithm applied to effective estimation of solar PV model parameters: A real-world practice. Neural Comput. Appl. 35 (18), 13529–13546.

Madhiarasan, M., Cotfas, D.T., Cotfas, P.A., 2022. Barnacles mating optimizer algorithm to extract the parameters of the photovoltaic cells and panels. Sensors 22 (18), 6989.

Mirjalili, S., Mirjalili, S.M., Lewis, A., 2014a. Grey wolf optimizer. Adv. Eng. Softw. 69, 46–61.

Mirjalili, S., Mirjalili, S.M., Lewis, A., 2014b. Grey wolf optimizer. Adv. Eng. Softw. 69, 46–61.

Mo, Y., Deng, X., Liu, P., Guo, J., Wang, W., Li, G., 2023. Insights into the application of carbon materials in heterojunction solar cells. Mater. Sci. Eng. R 152, 100711.

Navarro, M.A., Oliva, D., Ramos-Michel, A., Haro, E.H., 2023. An analysis on the performance of metaheuristic algorithms for the estimation of parameters in solar cell models. Energy Convers. Manage. 276, 116523.

Nicaire, N.F., Steve, P.N., Salome, N.E., Grégroire, A.O., 2021. Parameter estimation of the photovoltaic system using bald eagle search (BES) algorithm. Int. J. Photoenergy 2021.

Nowsherwan, G.A., Zaib, A., Shah, A.A., Khan, M., Shakoor, A., Bukhari, S.N.S., Riaz, M., Hussain, S.S., Shar, M.A., Alhazaa, A., 2023. Preparation and numerical optimization of TiO2: CdS thin films in double perovskite solar cell. Energies 16 (2), 900.

Nyamathulla, S., Chittathuru, D., 2023. A review of multilevel inverter topologies for grid-connected sustainable solar photovoltaic systems. Sustainability 15 (18), 13376.

Nyamathulla, S., Chittathuru, D., Muyeen, S., 2023. An overview of multilevel inverters lifetime assessment for grid-connected solar photovoltaic applications. Electronics 12 (8), 1944.

Pant, M., Zaheer, H., Garcia-Hernandez, L., Abraham, A., et al., 2020. Differential evolution: A review of more than two decades of research. Eng. Appl. Artif. Intell. 90, 103479.

Prasad, P.A.V., Dhanamjayulu, C., 2021. P&O MPPT integrated PV fed 15-level multi-level inverter. In: 2021 Innovations in Power and Advanced Computing Technologies. (I-PACT), IEEE, pp. 1–08.

Rao, R.V., Savsani, V.J., Vakharia, D., 2012. Teaching–learning-based optimization: An optimization method for continuous non-linear large scale problems. Inf. Sci. 183 (1), 1–15.

Rathod, A.A., Subramanian, B., 2022. Scrutiny of hybrid renewable energy systems for control, power management, optimization and sizing: Challenges and future possibilities. Sustainability 14 (24), 16814.

Rauf, H.T., Bangyal, W.H.K., Lali, M.I., 2021. An adaptive hybrid differential evolution algorithm for continuous optimization and classification problems. Neural Comput. Appl. 33 (17), 10841–10867.

Reddy, K., Saha, A.K., 2022. A modified whale optimization algorithm for exploitation capability and stability enhancement. Heliyon 8 (10).

Salgotra, R., Singh, U., Saha, S., Gandomi, A.H., 2020a. Self adaptive cuckoo search: Analysis and experimentation. Swarm Evol. Comput. 100751.

Salgotra, R., Singh, U., Saha, S., Gandomi, A.H., 2021a. Self adaptive cuckoo search: analysis and experimentation. Swarm Evol. Comput. 60, 100751.

Salgotra, R., Singh, U., Sharma, S., 2020b. On the improvement in grey wolf optimization. Neural Comput. Appl. 32 (8), 3709–3748.

Salgotra, R., Singh, U., Singh, S., Mittal, N., 2021b. A hybridized multi-algorithm strategy for engineering optimization problems. Knowl.-Based Syst. 217, 106790.

Sharma, P., Naidu, R.C., 2022. Optimization techniques for grid-connected pv with retired ev batteries in centralized charging station with challenges and future possibilities: A review. Ain Shams Eng. J. 101985.

Sharma, P., Raju, S., 2023a. Efficient estimation of PV parameters for existing datasets by using an intelligent algorithm. Optik (ISSN: 0030-4026) 171467.

Sharma, P., Raju, S., 2023b. Metaheuristic optimization algorithms: A comprehensive overview and classification of benchmark test functions. Soft Comput. 1–64.

Sharma, P., Reddy Salkuti, S., Kim, S.-C., 2022a. Advancements in energy storage technologies for smart grid development. Int. J. Electr. Comput. Eng. 12, 3421.

Sharma, P., Thangavel, S., Raju, S., Prusty, B.R., 2022b. Parameter estimation of solar PV using ali baba and forty thieves optimization technique. Math. Probl. Eng. 2022, 1–17.

Sharma, P., Thangavel, S., Raju, S., Prusty, B.R., et al., 2022c. Parameter estimation of solar PV using ali baba and forty thieves optimization technique. Math. Probl. Eng. 2022.

Storn, R., 1995. Differential evolution-a simple and efficient adaptive scheme for global optimization over continuous spaces, technical report. Int. Comput. Sci. Inst. 11.

Storn, R., Price, K., 1997. Differential evolution–A simple and efficient heuristic for global optimization over continuous spaces. J. Glob. Optim. 11 (4), 341–359.

Venkateswari, R., Rajasekar, N., 2021. Review on parameter estimation techniques of solar photovoltaic systems. Int. Trans. Electr. Energy Syst. 31 (11), e13113.

Wei, Z., Huang, C., Wang, X., Zhang, H., 2019. Parameters identification of photovoltaic models using a novel algorithm inspired from nuclear reaction. In: 2019 IEEE Congress on Evolutionary Computation. (CEC), IEEE, pp. 210–218.

Wolpert, D.H., Macready, W.G., 1997. No free lunch theorems for optimization. IEEE Trans. Evol. Comput. 1 (1), 67–82.

Wu, F., Zhang, J., Li, S., Lv, D., Li, M., 2022. An enhanced differential evolution algorithm with bernstein operator and refracted oppositional-mutual learning strategy. Entropy 24 (9), 1205.

Xiong, G., Li, L., Mohamed, A.W., Yuan, X., Zhang, J., 2021. A new method for parameter extraction of solar photovoltaic models using gaining-sharing knowledge based algorithm. Energy Rep. 7, 3286–3301.

Xiong, G., Zhang, J., Shi, D., He, Y., 2018a. Parameter extraction of solar photovoltaic models using an improved whale optimization algorithm. Energy Convers. Manage. 174, 388–405.

Xiong, G., Zhang, J., Shi, D., He, Y., 2018b. Parameter identification of solid oxide fuel cells with ranking teaching-learning based algorithm. Energy Convers. Manage. 174, 126–137.

Xiong, G., Zhang, J., Shi, D., Yuan, X., 2019. Application of supply-demand-based optimization for parameter extraction of solar photovoltaic models. Complexity 2019, 1–22.

Yang, X.-S., 2012. Flower pollination algorithm for global optimization. In: International Conference on Unconventional Computing and Natural Computation. Springer, pp. 240–249.

Yang, X.-S., Karamanoglu, M., He, X., 2013. Multi-objective flower algorithm for optimization. Procedia Comput. Sci. 18, 861–868.

Yang, C., Su, C., Hu, H., Habibi, M., Safarpour, H., Khadimallah, M.A., 2023. Performance optimization of photovoltaic and solar cells via a hybrid and efficient chimp algorithm. Sol. Energy 253, 343–359.

Zhi, C., Wang, S., Sun, S., Li, C., Li, Z., Wan, Z., Wang, H., Li, Z., Liu, Z., 2023. Machine-learning-assisted screening of interface passivation materials for perovskite solar cells. ACS Energy Lett. 8 (3), 1424–1433.